

A new microphysiological system shows hypoxia primes human ISCs for interleukin-dependent rescue of stem cell activity

Kristina R. Rivera^{1*}, R. Jarrett Bliton^{1*}, Joseph Burclaff¹, Michael J. Czerwinski², Jintong Liu², Jessica M. Trueblood⁵, Caroline M. Hinesley⁵, Keith A Breau², Shlok Joshi², Vladimir A. Pozdin³, Ming Yao⁴, Amanda L. Ziegler⁵, Anthony T. Blikslager⁵, Michael A. Daniele^{1,3} and Scott T. Magness^{1,2,6**}

[1] Joint Department of Biomedical Engineering, North Carolina State University and University of North Carolina at Chapel Hill 911 Oval Dr., Raleigh, NC, 27695 (USA)

[2] Department of Cell Biology & Physiology, University of North Carolina at Chapel Hill, Chapel Hill, NC, 27599 (USA)

[3] Department of Electrical & Computer Engineering, North Carolina State University, Raleigh, NC, 27695 (USA)

[4] Department of Mechanical & Aerospace Engineering, North Carolina State University, Raleigh, NC 27695 (USA)

[5] Center for Gastrointestinal Biology and Disease, College of Veterinary Medicine, North Carolina State University, Raleigh, North Carolina

[6] School of Medicine, University of North Carolina at Chapel Hill, Chapel Hill, NC, 27599 (USA)

[*] Equal contribution

[**] Correspondence: magness@med.unc.edu

1 ABSTRACT

2 **Background & Aims:** Hypoxia in the intestinal epithelium can be caused by acute ischemic events or
3 conditions like Inflammatory Bowel Disease (IBD) where immune cell infiltration produces ‘inflammatory
4 hypoxia’, a chronic condition that starves the mucosa of oxygen. Epithelial regeneration after ischemia
5 and IBD suggests intestinal stem cells (ISCs) are highly tolerant to acute and chronic hypoxia; however,
6 the impact of acute and chronic hypoxia on human ISC (hISC) properties have not been reported. Here
7 we present a new microphysiological system (MPS) to investigate how hypoxia affects hISCs isolated
8 from healthy human tissues. We then test the hypothesis that some inflammation-associated
9 interleukins protect hISCs during prolonged hypoxia.

10 **Methods:** hISCs were exposed to <1.0% oxygen in the MPS for 6-, 24-, 48- & 72hrs. Viability, HIF1 α
11 response, transcriptomics, cell cycle dynamics, and hISC response to cytokines were evaluated.

12 **Results:** The novel MPS enables precise, real-time control and monitoring of oxygen levels at the cell
13 surface. Under hypoxia, hISCs remain viable until 72hrs and exhibit peak HIF1 α at 24hrs. hISCs lose
14 stem cell activity at 24hrs that recovers at 48hrs of hypoxia. Hypoxia increases the proportion of hISCs
15 in G1 and regulates hISC capacity to respond to multiple inflammatory signals. Hypoxia induces hISCs
16 to upregulate many interleukin receptors and hISCs demonstrate hypoxia-dependent cell cycle
17 regulation and increased organoid forming efficiency when treated with specific interleukins

18 **Conclusions:** Hypoxia primes hISCs to respond differently to interleukins than hISCs in normoxia
19 through a transcriptional response. hISCs slow cell cycle progression and increase hISC activity when
20 treated with hypoxia and specific interleukins. These findings have important implications for epithelial
21 regeneration in the gut during inflammatory events.

22 KEYWORDS

23 Inflammatory Hypoxia; Intestinal stem cells; Stem Cell Priming; Oxygen Sensor; Cytokines

24 **ABBREVIATIONS**

| | |
|----|---|
| 25 | Inflammatory Bowel Disease (IBD) |
| 26 | Intestinal stem cell (ISC) |
| 27 | Human intestinal stem cell (hISC) |
| 28 | Microphysiological system (MPS) |
| 29 | integrated Phosphorescent Oxygen Biosensor (iPOB) |
| 30 | Near Infrared (NIR) |
| 31 | 2-Dimensional (2D) |
| 32 | Occludin (OCLN) |
| 33 | organoid forming efficiency (OFE) |
| 34 | CellRaft™ Arrays (CRAs) |
| 35 | Principal Component Analysis (PCA) |
| 36 | Principal Component (PC) |
| 37 | Gene Set Enrichment Analysis (GSEA) |
| 38 | interleukin (IL) |
| 39 | Differential gene expression (DGE) |
| 40 | endoplasmic reticulum (ER) |
| 41 | unfolded-protein response (UPR) |
| 42 | Innate Lymphoid Cells Type 2 (ILC2s) |
| 43 | dithiothreitol (DTT) |
| 44 | Expansion Media (EM) |
| 45 | polymethylmethacrylate (PMMA) |
| 46 | dichloromethane (DCM) |
| 47 | poly(2-hydroxyethyl methacrylate) (pHEMA) |
| 48 | Fluorescence-activated cell sorting (FACS) |
| 49 | RNA integrity number (RIN) |
| 50 | integrated fluidic circuits (IFCs) |

51 INTRODUCTION

52 Cellular respiration in complex multi-layered tissues relies on a constant supply of oxygen to
53 maintain healthy physiologic states. To this end, the intestinal epithelium maintains physiologic oxygen
54 tension through a highly vascularized tissue that is perfused by a vast network of vessels that terminate
55 in capillary beds where oxygen is released to adjacent cells in a local microenvironment.¹ In the crypt-
56 villus epithelial architecture, cells can experience marked differences in physiologic oxygen
57 concentrations where crypt-based cells experience higher oxygen levels compared to cells at the villus
58 tips.² Along the crypt-villus axis, a steep oxygen gradient is present wherein microenvironments that
59 are separated by just ~100 cell distances experience a ~10-fold lower oxygen concentration.³ While
60 lower oxygen concentrations within the gradient are tolerated as normal, sudden or dramatic changes
61 in the magnitude and duration of oxygen loss can lead to pathological hypoxia resulting in cell
62 dysfunction and/or death.⁴

63 Most studies that evaluate the impact of tissue oxygen deprivation do so in the context of
64 ischemia-reperfusion injury. This is characterized by an initial ischemic event such as bowel
65 strangulation, aneurysm, or organ harvest for transplantation which induces hypoxia. Subsequent
66 reperfusion of blood flow, and thus oxygen, induces a separate type of oxidative injury caused by free
67 radicals and reactive oxygen species.^{5,6} Hypoxic events can be categorized as acute, which are
68 typically transient events that last on the order of minutes to hours, and chronic hypoxic events that last
69 much longer, for at least 24 hours or more.⁷ Inflammatory hypoxia, a type of chronic hypoxia, is caused
70 by the presence of large numbers of immune cells in the submucosal compartment depleting local
71 oxygen supplies.^{4,8,9} Following epithelial injury, a massive influx of immune cells is recruited to prevent
72 pathogens and other luminal contents from causing further damage. This massive influx of immune
73 cells consumes the local oxygen supply to the epithelium^{4,10-13} and can cause vasoconstriction, which
74 further starves the epithelial cells of oxygen.^{3,14,15} Hypoxia due to inflammation can exist in isolated
75 microenvironments that might initially go unnoticed and eventually resolve themselves. However,
76 longer periods of inflammation, such as in Inflammatory Bowel Disease (IBD) may compromise the
77 epithelium and normal repair mechanisms ultimately resulting in, or contributing to, mucosal erosions
78 and ulcerations.^{8,12} Consistent with this concept, inflammatory responses have been shown to produce
79 localized and chronic hypoxic episodes in the intestinal stem cell (ISC) zone, potentially leading to
80 impaired ISC survival, renewal, and differentiation, ultimately impeding mucosal repair and producing
81 ISC death.^{6,15,16}

82 While numerous studies focus on the impact of hypoxia on repair mechanisms involving
83 restitution in differentiated enterocytes^{6,17-21} few studies investigate the impact of hypoxia on ISC
84 properties and ISC-dependent repair mechanisms²², especially in human tissues. Traditionally, human
85 cancer cell lines are used to study acute and chronic hypoxia at the cellular level but transformed cells
86 exhibit abnormal proliferation and cell death dynamics and they do not properly differentiate, thus they
87 are poor models of human ISCs (hISCs).²³ Studies in porcine small intestines show that the so-called
88 'reserve' ISC (rISC) exhibits high tolerance to hypoxic episodes of up to 4 hours of
89 hypoxia/ischemia^{15,22}, but these studies do not evaluate the impact of chronic hypoxia on hISCs. A
90 highly physiologically relevant human model to study acute ischemia was developed²⁴ and while the
91 study primarily characterizes the differentiated epithelium under hypoxia, a lack of apoptosis in the crypt
92 observed after 45 min of ischemia indicates hISCs are highly resistant to short hypoxic episodes.²⁰
93 Despite the important observations and advances outlined in these in vivo studies, all have been
94 performed either in the context of ischemia-reperfusion injury, precluding the evaluation of hypoxic
95 injury uncoupled from reperfusion injury, or performed under short-duration ischemic conditions (<4
96 hours), and thus interpretations are limited to acute rather than chronic hypoxia injury.

Investigating the impact of hypoxia on hISCs has been historically limited by the inability to indefinitely culture hISCs, the lack of high-resolution in vitro platforms where oxygen levels can be tuned and accurately monitored in real time, and ethical considerations of human research that preclude in vivo experimentation. In this study, we engineered a microphysiological system (MPS) that delivers multiple durations and magnitudes of hypoxia to primary hISCs. The MPS allows for precise remote monitoring and control of oxygen concentrations in real-time at the cell surface interface. We use the MPS to create controlled durations of acute and chronic hypoxic episodes and evaluate dynamic transcriptomic changes within hISCs under these conditions. We focused our evaluation on chronic hypoxic events related to hISC-immune cell cross talk through interleukin signaling that might occur during inflammatory hypoxia. Our findings have broad implications for understanding the role in which inflammatory hypoxia can impact hISC behavior in gross clinical presentation of ischemia-reperfusion injury and focal ischemic events that occur in Inflammatory Bowel Disease-related hypoxia.

RESULTS

A new microscopy-compatible microphysiological system enables precise regulation and real-time monitoring of oxygen levels at the cell-media interface.

To address the limitations of sensitivity, accuracy and scale in existing environmental culture systems that create a hypoxic environment, we developed a novel MPS the size of a standard microscope slide where oxygen tension could be tailored to precise levels. The MPS design consists of 2 major structural components, 1) the 3D-printed light- and air-tight container required for phosphorescence detection and hypoxia induction in the closed system and 2) a clear-bottomed acrylic five-well tissue culture plate with each well containing a hydrogel scaffold that facilitates hISC expansion, which all sits inside of the sealed chamber²⁵ (**Fig. 1A,B**, see methods).

The MPS was designed as a closed system in which ambient air flowed over each well via continuous delivery of mixed gases. A biocompatible integrated Phosphorescent Oxygen Biosensor (iPOB) was placed on the hydrogel scaffold surface to provide real-time oxygen measurements specifically at the cell surface interface (**Fig. 1C**)²⁶. Oxygen levels were quantified by the iPOB using Near Infrared (NIR) phosphorescence lifetime fluorimetry which measures the oxygen-dependent decrease in phosphorescence lifetime to determine local oxygen concentration (**Fig. 1C,D**)²⁷. The iPOBs are reusable, highly sensitive, and capable of detecting a broad range of oxygen levels created by an off-chip gas mixer²⁸ (**Fig. 1D**, see methods).

The MPS design facilitates easy access to refresh media, add compounds, and perform a variety of downstream assays including microscopy, transcriptomic analysis, and immunostaining. The MPS is fabricated from relatively inexpensive commercially available materials and can be sterilized and reused many times. Notably, multiple MPSs can be connected to the same gas source to accommodate complex experimental designs that require many perturbations and technical replicates (see methods). Together, these demonstrate an ideal model system for evaluating the effect of hypoxia on hISCs.

The MPS supports culture of hISC/progenitor epithelial monolayers

We recently developed methods that support indefinite 2-Dimensional (2D) expansion of proliferative human intestinal stem cells from primary small intestine and colon²⁵. Under normoxic conditions (i.e., 37°C, 5% CO₂, and remainder atmospheric air), hISC monolayers can be cultured on a defined hydrogel and media formulation that supports hISC expansion while repressing differentiation^{25,29}. This method was used to expand primary jejunal hISCs isolated from small intestinal

crypts of an organ transplant donor and then transferred to the MPS. Initial characterization of the proliferative hISC monolayer was performed in the MPS under normoxic conditions by immunostaining. The monolayers demonstrated DNA synthesis as measured by S-phase marker EdU, expression of hISC/progenitor cell marker SOX9^{30,31}, and epithelial cell tight junction protein Occludin (OCLN) (**Fig. 1E**). These results demonstrate the MPS is biocompatible with primary hISCs that are consistent with proliferating hISC/progenitor cell populations.

Next, the baseline functional stemness of proliferative hISCs cultured on the MPS under normoxia was evaluated. hISCs were cultured on the MPS as proliferative monolayers under atmospheric O₂ levels, dissociated to single cells and plated in Matrigel™ on a CellRaft™ Array to assess organoid forming efficiency (OFE), a measure for in vivo hISC activity³²⁻³⁴. Single cells in the microwells were identified, quantified, and putative hISCs were individually tracked over a 6-day culture period to determine whether an organoid formed. The data demonstrate ~4% of single cells cultured in the MPS under hISC expansion conditions generated an organoid at each time point measured (2, 4, and 6 days after plating) (**Fig. 1F**), which is consistent with OFE of FACS-isolated hISCs from a Lgr5-EGFP expressing reporter gene mouse and also consistent with human organoid-derived hISCs cultured for the same period of time in synthetic matrices^{34,35}. These findings demonstrate that hISCs cultured as 2D monolayers on the MPS maintain hISC properties over time, and at similar ratios to those observed in vivo and in 3D organoid systems.

To define the speed at which severe hypoxia could be achieved and maintained in the MPS, an iPOB was added to the epithelial cell surface, and real-time oxygen levels at the cell-media interface were measured for 24 hours (**Fig. 1G, inset**). Oxygen concentrations of <1% (below 10 μM) are considered severely hypoxic but not anoxic³⁶. The data show the MPS produced a rapid hypoxic environment of 0.3% O₂ (3 μM) within ~30 minutes, which was constantly maintained during the 24-hour experiment (**Fig. 1G**). Interestingly, when proliferative hISC monolayers were cultured in normoxic conditions as a control, cellular respiration reduced oxygen levels at the cell-media interface from 18% (180 μM) to 3.5% (35 μM) in the MPS. These data demonstrate that physiologic O₂ metabolism of proliferative hISCs produce a steady-state flux of O₂ in just 30-minutes that is 5-fold less than atmospheric oxygen levels.

Human ISC monolayer cultures demonstrate peak HIF1 α response at 24 hours of severe hypoxia with no loss of stem cell activity after 48 hours of severe hypoxia

The HIF1 α transcription factor¹³ is a master regulator of the hypoxic response conserved across all tissues and species.^{14,37} Under normoxia, HIF1 α is constitutively expressed but is immediately targeted for degradation¹⁴. By contrast, under hypoxia, HIF1 α degradation is inhibited through well-established mechanisms, resulting in rapid accumulation and regulation of a broad range of downstream target genes that regulate cell survival, proliferation, metabolism, and cell migration^{13,38}. Immunostaining for HIF1 α in hISCs under durations of hypoxia shows a significant accumulation of HIF1 α only at 24 hours of severe hypoxia (**Fig. 2A,B**). No significant change in HIF1 α was observed at 6 hours of hypoxia compared to normoxia, which may indicate tolerance of proliferative hISCs to shorter hypoxic episodes. Lack of HIF1 α accumulation at 48 hours of hypoxia is likely due to known dampening of the HIF-response that occurs after cells re-equilibrate to tolerate new and sustained low O₂ levels.⁴ Interestingly, hISCs cultured under normoxia showed a significant increase in HIF1 α levels 24 hours after media change when compared to the 6 hour normoxic samples. This minor hypoxic response is consistent with previous observations that cells in submersion cultures experience a localized hypoxic environment due to the slower rate of diffusion of O₂ through medium relative to the

rate of consumption in cellular metabolism.³⁹ Together, these findings established a timeframe for further investigation into the mechanisms by which hISCs resist death and preserve functional stemness and viability in response to HIF1 α accumulation in hISCs during short-, medium-, and long-term hypoxia.

To confirm whether proliferative hISCs in the MPS were experiencing a HIF-response at 0.3% O₂, qPCR was performed to detect expression of canonical HIF1 α target genes that are typically upregulated during hypoxia. After 24 hours of hypoxia, *HIF1 α* demonstrated little transcriptional change as expected since its activity is mediated by post-transcriptional stabilization (**Fig 2C**)^{40,41}. By contrast, the set of classic HIF1 α target genes (*VEGF*, *SCL2A1/GLUT1*, *BCL2*, *BNIP3*) were all significantly upregulated compared to normoxic controls (**Fig. 2C**)⁴²⁻⁴⁴. These findings demonstrate that an O₂ tension of 0.3% (3 μ M) for 24 hours is sufficient to activate a canonical hypoxia response inside proliferative hISCs.

Next, we sought to explore the extent to which hISCs can survive severe hypoxia. hISCs were exposed to severe hypoxia (<1% O₂ as measured by the iPOB) in the MPS for 6, 24, 48, or 72 hours and viability was evaluated by staining for early apoptosis marker, Annexin V (**Fig. 2D**)⁴⁵. Flow cytometric quantification of Annexin V negative cells demonstrates ~90% viability through 48 hours of severe hypoxia. However, at 72 hours of severe hypoxia, there was a significant decrease in viability as measured by Annexin V-negative staining, from ~90% viable in normoxic controls to ~70% viable after 72 hours of hypoxia.

To determine how longer episodes of hypoxia would impact hISC activity, monolayers were exposed to 24 hours or 48 hours of hypoxia or normoxia as a control in the MPS. At 24 and 48 hours of hypoxia, hISCs demonstrate persistent expression of the proliferation marker, KI67, albeit nuclear KI67 levels are reduced at 48 hours of hypoxia (**Fig 2E**). To quantify hISC activity after these durations of hypoxia, monolayers were subjected to 24 or 48 hours hypoxia, dissociated to single cells, and then applied to CellRaft™ Arrays (CRAs) for high-throughput accurate quantification of clonal OFE.³⁴ CRAs enable up to ~10,000 hISCs to be plated in microwells on a small device and individual hISCs can be evaluated for OFE over time^{34,46}. After 24 hours of hypoxia OFE decreased ~2.5-fold (**Fig. 2F**). Interestingly, when hISCs were exposed to a longer 48-hour hypoxia duration, the OFE was indistinguishable from normoxia controls suggesting hypoxia-induced survival mechanisms were invoked in hISCs after 24 hours of hypoxia (**Fig. 2G**).

To evaluate the time-dependent gene expression changes occurring in response to hypoxia and HIF1 α accumulation, RNA-sequencing was performed on proliferative hISCs cultured under normoxia and severe hypoxia for 6, 24, and 48 hours (**Fig. 2H**). Principal Component Analysis (PCA) demonstrated high agreement between technical replicates (n = 3) for each timepoint and revealed global transcriptomic changes in hISCs between normoxic and hypoxic samples. The 6-hour and 48-hour normoxic samples clustered closely on the first Principal Component (PC), whereas the 24-hour normoxic samples deviated from the other normoxic samples on the first PC. Interestingly, the 48-hour normoxic samples deviated from the 6-hour normoxic samples on the second axis, which is consistent with our previous data that hISCs mount a transient HIF-response at 24 hours following media change that resolves after 48 hours in culture (**Fig 2A,B**). These results suggest that normoxic hISCs experience a minor hypoxic event following media change that results in a subtle, but meaningful, shift in gene expression profile in line with a hypoxic response and that following this shift, the hISCs return to a slightly altered gene expression profile.

226 For hypoxic samples, the 6-hour samples clustered closest to the 24-hour normoxic samples,
227 which is consistent with the previous observation that the 24-hour normoxic hISCs were undergoing a
228 minor HIF-response. By contrast, the 24-hour and 48-hour hypoxic samples clustered together but
229 deviated significantly from all other samples on the first PC, indicating the onset of a strong HIF-
230 response in hISCs at 24 hours of severe hypoxia that persists through 48 hours of hypoxia. The
231 transcriptomic shift at 24 hours of hypoxia is aligned with the robust HIF1 α accumulation and significant
232 decrease in OFE after 24 hours of hypoxia, reinforcing the concept that hISCs tolerate shorter periods
233 of hypoxia through at least 6 hours but require transcriptional changes at 24 hours to regain organoid
234 forming activity at 48 hours (**Fig. 2F,G**).

235 To determine if durations of severe hypoxia promoted differentiation, transcriptomic analysis was
236 performed to evaluate the expression of hallmark lineage markers for hISCs and main classes of
237 differentiated cells (**Fig 2I**).^{47,48} Consistent with decreased OFE at 24 hours of hypoxia, hISCs show
238 decreased expression of stem and progenitor marker genes. Interestingly, this decreased expression
239 continues through 48 hours of hypoxia, even though OFE is restored to normoxic levels, which is
240 consistent with the changes seen in our PCA (**Fig 2H**). The data show very low expression and no
241 appreciable trends in hypoxia-associated changes of genetic markers for Absorptive Enterocytes (ALPI,
242 SI) and secretory lineages, Paneth- (DEFA5), Enteroendocrine- (CHGA, CHGB), Tuft- (PTGS1),
243 Goblet- (MUC2), and BEST4 cells (BEST4) compared to markers of proliferative hISCs and progenitor
244 cells. These data indicate that hypoxia alone does not promote differentiation of hISCs.

245 ***Hypoxia primes an hISC transcriptional state to respond to extrinsic interleukin signals and*** 246 ***intrinsic downstream mediators of inflammation.***

247 To investigate the potential molecular and physiological context associated with these time-
248 dependent transcriptomic changes, Gene Set Enrichment Analysis (GSEA) (**Fig. 3A**) was used to
249 evaluate the comprehensive gene expression changes observed in our RNA sequencing data. GSEA
250 demonstrates that the hypoxia-related gene set is highly enriched at all timepoints compared to
251 controls, providing confidence in the pathway-based analysis tools^{49,50} GSEA findings indicate hISC
252 monolayers regulate a subset of pathways consistently across all hypoxia durations while other
253 pathways are regulated in a dynamic manner. Specifically, transcriptomic analyses on hISC
254 monolayers revealed enriched gene sets for inflammatory signaling through specific interleukin-
255 mediated pathways, (e.g., Inflammatory Response, IL6 JAK STAT3 Signaling, IL2 STAT5 Signaling,
256 and INF α/γ Responses) (**Fig. 3A**).

257 Within the gene set for 'Hallmark Inflammatory Response' ~4.5% of the genes (8/184) were
258 interleukin (IL) receptors and all demonstrated some form of hypoxia-dependent regulation, thus we
259 focused our analysis on all IL receptors^{4,10,14} with the goal of revealing how hypoxia-related
260 inflammatory conditions might extrinsically signal to hISCs (**Fig. 3B**). Interleukins and their cognate
261 receptors have well established roles in regulating stem cell proliferation in diverse tissue types⁵¹⁻⁶⁰. Of
262 45 IL receptors, 91% had detectable expression across all durations of hypoxia. Differential gene
263 expression (DGE) between normoxic and hypoxic environments revealed a subset of 13 IL receptors
264 (IL1R1, IL1R2, IL1RAP, IL1RAPL1, IL2RG, IL4R, IL11RA, IL13RA1, IL17RA, IL17RC, IL17RE, IL18R1,
265 IL20RA) that were regulated by hypoxia in a time-dependent fashion, potentially indicating specific roles
266 during early (6 hours), mid (24 hours), and late (48 hours) durations of severe hypoxia.

267 To compare hypoxia-dependent changes in IL receptor expression, we looked at fold change
268 differences in gene expression for the 45 IL receptor genes observed in our dataset. IL1RAPL1, IL1R2,

IL10RB, IL22RA1, IL6R, IL11RA, IL17RE, IL1RN, IL2RG, IL4R, IL17RA, and IL17RB were considered early responders, as all showed hypoxia-dependent up- or down-regulated expression at 6 hours (**Fig 4A**). Of the early responders IL1RN, IL6R, IL10RB, IL17RB, and IL22RA1 were considered early persistent responders as their hypoxia-dependent expression changes were consistent through 24 and 48 hours of hypoxia (**Fig 4A-C**). IL1RAP, IL1R1, IL18R1, and IL20RA were considered mid-responders as their regulation patterns changed beginning at 24 hours of hypoxia. Of these, only IL1RAP had significant change in regulation through 48 hours. IL13RA1 and IL17RC were considered late responders as their hypoxia-dependent gene expression patterns were only observed following 48 hours of hypoxia. IL1R2 and IL11RA were considered dynamic responders as their expression patterns changed at 6 and 48 hours of hypoxia. The significant trends were verified by qPCR for the subset of IL receptors that were consistently upregulated (IL6R, IL10RB, IL22RA1) or downregulated (IL17RB) (**Fig. 4D**). To confirm that hISCs expressed the IL receptors in vivo and in the MPS culture system, we compared IL receptor expression from our recent single cell transcriptomic atlas of the human intestine to single cell transcriptomic dataset for hISCs cultured as monolayers in media that supports hISC expansion (**Fig. 4E,F**).^{48,61} The data show that all members of the subset of hypoxia-regulated IL receptors have measurable expression in hISCs both in vivo and in vitro. These results show hISC undergo time-dependent changes in IL receptor expression during acute and chronic hypoxic events that primes hISCs to respond to extrinsic inflammatory signals.

Hypoxia increases proportion of hISCs residing in G1 phase

As a baseline, in the absence of interleukins, we determined the impact of hypoxia on regulating proliferation and cell cycle phases (**Fig 5A**). hISC monolayers were pulsed with EdU for the last 2 hours of culture to quantify cells in S-phase during normoxia or hypoxia, then co-stained for general cell-cycle marker KI67 (**Fig 5B**). Individual nuclei were segmented using Cellpose and the percent of cells in S-phase (EdU⁺) or in any cell cycle phase (KI67⁺) were quantified.^{62,63} Confocal images were used to train the algorithm for precise nuclear segmentation (Bisbenzimidazole+). Approximately 150,000 nuclei were automatically identified (i.e., segmented) across all experimental conditions (**Fig 5B**).^{62,63} After segmentation, KI67 and EdU channels were overlaid onto the automatically segmented nuclei to quantify the mean fluorescence intensity and percent of cells positive for each cell cycle marker on a per-nuclei and per-colony basis. The number of cells in mitosis (M-phase) were evaluated by counting condensed chromosomes that were stained by KI67 and morphologically identifiable (**Fig 5C**).

To determine whether hypoxia caused a specific arrest or delay in any particular cell cycle phase, we leveraged a recent study which shows that KI67 expression levels can reliably predict cell cycle phases.⁶⁴ KI67 levels can serve as a marker for cell cycle progression and exit, with the lowest levels of KI67 in G1/G0 phase, intermediate levels during S-phase, and highest levels in G2/M phase⁶⁴. We evaluated the levels of KI67 in hISCs for segmented nuclei from ~38,000 cells and found that severe hypoxia significantly decreased KI67 under severe hypoxia (**Fig. 5D**). Hypoxic hISC cultures showed approximately 67.2% of cells undergoing cell cycling (KI67⁺), a significant decrease compared normoxic conditions where 78.9% of cells reside in the cell cycle (**Fig 5E**).⁶⁴ More granular analysis revealed reductions in the number of cells in S-phase (EdU⁺) and M-phase (mitotic bodies) (**Fig 5E**). The lower levels of KI67, combined with the significant decrease in S- and M-phase cells, suggests that 24 hours of severe hypoxia likely causes either G1 arrest or lengthening of G1. Transcriptomic data does not show increases in differentiated lineage markers (**Fig. 2I**) indicating that hypoxia is not pushing hISCs to differentiate as they exit the cell cycle. Together, these findings demonstrate that over 24 hours of hypoxia, hISCs negatively regulate progression through the cell cycle and that hypoxia likely promotes G1 dormancy in hISCs.

Hypoxia alters hISC cell cycle regulation by specific interleukins

We next explored whether the hypoxia-regulated IL receptors could impact hISC cell cycle when in the presence of their cognate interleukins: IL1 α , IL1 β , IL2, IL4, IL6, IL10, IL13, IL17^{AF} (heterodimer), IL22, and IL25. hISC monolayers were treated with ILs under normoxia or hypoxia for 24 hours, to simulate ILs that might be present during an chronic inflammatory response, before fixing, staining, and imaging^{8,12,65-68}. No ILs caused significant impacts on the total proportion of proliferating cells (KI67⁺) after 24 hours of hypoxia; however, at 24 hours of normoxia or hypoxia, hISCs shift cell cycle phase dynamics in response to interleukin signals (**Fig 6A-F**). IL1 α increases the proportion of hISCs in S-phase in normoxia, but this effect is largely abrogated in hypoxic hISCs (**Fig 6A**). IL2, IL4, and IL25 significantly increase the percentage of hISCs in M-phase only in hypoxia, with no change noted in normoxia (**Fig 6B-E**); whereas IL22 affects normoxic hISCs, but not hypoxic (**Fig 6F**). IL6, IL10, IL13, and IL17^{AF} had no effects on cell cycle phase dynamics (**Fig. 7A-D**). The IL1 α -dependent decrease in S-phase cells with no increase in M-phase hISCs suggests that IL1 α further promotes G1 arrest or elongation under hypoxia, thereby reducing observable S-phase cells. IL2, IL4, and IL25-dependent increases in M-phase hISCs with no observable decrease in KI67⁺ cells suggest slow progression of hISCs through M-phase under hypoxic conditions. These indicate that hypoxia primes hISCs to respond to ILs differently than hISCs in normoxia

Hypoxia affects hISC activity in response to interleukin treatment

While the previous experiments were designed to focus on the impact of hypoxia-dependent IL receptor priming on proliferation dynamics, we next sought to probe whether this IL receptor priming would regulate stem cell activity in the presence of cognate interleukins. hISC monolayers were exposed to 24 hours of normoxia or severe hypoxia, then dissociated to single hISCs and plated in conventional 3D organoid assays to evaluate OFE of clonal hISCs in the absence or presences of ILs (**Fig 8A**). Similar to OFE assays in the CellRaft arrays (**Fig 2F**), we found that hypoxia induced a decrease in OFE at 24 hours (**Fig. 8B,C**). IL6, IL10, and IL13 (**Fig 8D-F**) increased OFE in a hypoxia-independent manner, while IL1 β , IL2, IL4, and IL25 demonstrated hypoxia-dependent increases in OFE (**Fig 8G-J**), thereby rescuing the negative impacts of hypoxia on hISC. No effects on OFE were observed for IL1 α , IL17^{AF}, and IL22 (**Fig 8K-M**). Together, these findings show 24 hours of hypoxia primes hISCs to respond to cognate ILs differently in hypoxia than in normoxia by altering cell cycle phase dynamics and in some cases enhancing hISC activity.

DISCUSSION

Human health conditions that cause loss of oxygen to the intestinal epithelium result in rapid loss of the differentiated cells, requiring quick regeneration from the stem cell pools located at the base of the crypts^{6,69,70}. Evaluating the impact of hypoxia on hISCs in vivo is challenging due to ethical considerations and the inability to precisely control many experimental variables. While in vitro systems are available to regulate ambient oxygen levels, these platforms are limited in that oxygen levels are monitored in large volume incubators and not localized to the cell-medium interface. Here we developed a flexible and oxygen-tunable MPS that addresses many limitations of conventional systems and represents a next-generation platform to study hypoxic injury across a broad range of cell and tissue types. While not explored in this study, the flexible design and small scale of the MPS will enable co-culture of hISC with other cell types, such as immune cells, which are key players in hypoxia-related intestinal conditions.

356 Murine intestinal epithelial monolayers were shown to experience repeated bouts of hypoxia
357 during conventional cell culture methods.³⁹ Upon media changes, oxygen levels were at saturation but
358 the levels substantially reduced in media over time, ostensibly by cellular metabolism, thereby creating
359 a hypoxic environment and inducing a HIF1 α response.³⁹ These observations indicate that oxygen
360 diffusion from ambient incubator gas mixes was insufficient to compensate for the oxygen metabolism
361 of mouse intestinal epithelial cells submerged in culture media.³⁹ Using our newly developed MPS that
362 supports 2D cultures of hISCs, we show similar findings in that fresh media at the cell surface interface
363 is saturated at about ~12% O₂ from atmospheric gasses and that hISCs metabolize O₂ levels in the
364 media from ~12% to ~3% in approximately 3 hours. At that point, O₂ levels stabilize but are sufficiently
365 low to induce a small but appreciable hypoxia-induced HIF1 α response after 24 hours of submersion
366 culture. Our findings challenge general assumptions regarding oxygen availability following regular
367 medium changes in many conventional cell culture systems. More specifically, our data suggest that
368 any cells cultured in submersion culture can experience unappreciated HIF1 α -dependent
369 transcriptional changes following media changes, confounding interpretations.

370 Our findings show that hISCs are highly resilient to severe hypoxia for up to 48 hours. There
371 was a decrease in functional hISC activity at 24 hours of hypoxia, but this resolved at 48 hours with no
372 significant difference in OFE compared to normoxic controls. Several studies in rodent and human
373 intestines highlight the role of endoplasmic reticulum (ER) stress and the unfolded-protein response
374 (UPR) during acute hypoxic episodes.^{39,71,72} The UPR is considered to mediate cell death by activating
375 the intrinsic apoptotic cascade; however, several more contemporary reports in the context of cancer
376 cell lines indicate that unresolved ER-stress, which can occur during long durations of hypoxia⁷³, can
377 induce necroptosis.⁷³⁻⁷⁵ We found no clear evidence of increased apoptosis during 48 hours of severe
378 hypoxia, and while necroptosis pathways were not evaluated, there was no decrease in hISC activity
379 at 48 hours of hypoxia, strongly supporting that other cell death pathways are being repressed in hISCs
380 through 48 hours of hypoxia.

381 Transcriptomic profiling of hISCs during chronic and severe hypoxia revealed enrichment of
382 regulated genes related to inflammation and inflammation responses. Among these genes we noticed
383 many cytokine/interleukin receptors were significantly regulated in a hypoxia-dependent manner. While
384 the interleukin responses mediated through these receptors impact many different aspects of cell
385 biology, we focused our analysis on how hypoxia-induced changes in hISC expression of IL receptors,
386 could impact cell cycle dynamics and stem cell activity through stimulation using their cognate ILs. In
387 the absence of ILs, the baseline hISC response to 24 hours of hypoxia was a significant decrease in
388 the overall number of cycling cells (KI67⁺) with notable reductions in numbers of cells in each phase of
389 the cell cycle. While the number of cycling cells was reduced at 24 hours of hypoxia based on KI67,
390 the lack of differentiated cell markers and absence of reduced OFE of hISCs at 48 hours suggests
391 hISCs do not exit cell cycle or differentiate as the result of severe hypoxia but rather enter a 'safe mode'
392 characterized by a reversible dormant state, reminiscent of a reserve ISC state⁷⁶. Further genetic and
393 molecular analysis will be necessary to reveal these mechanisms.

395 During inflammatory hypoxia, local immune cells express a complex mixture of ILs near hISCs.⁸
396 In our model, hypoxia primed hISCs to respond to subsets of ILs by regulating cognate IL receptors.
397 Stimulation of hypoxia-regulated IL receptors by their cognate ILs produced notable hypoxia-dependent
398 increases in G2/M-phase cells for IL2, IL4, and IL25 that generally rescued the baseline hypoxia-
399 dependent loss of G2/M-phase cells. Less notable, IL1 α caused a modest but significant reduction in
400 S-phase cells. There is a collection of studies describing how IL2 and IL4 promote proliferation in
401 immune cells^{53,56,77,78}, and studies in colon and pancreatic cancer cells demonstrate that IL4 enhances
402 proliferation^{79,80}, but we found no studies describing the role of these ILs on mouse or human ISCs.
403 IL25 is expressed by tuft cells during parasitic worm infections.⁸¹⁻⁸⁴ Secreted IL25 interacts with the
404 cognate heterodimer receptors, IL17RA and IL17RB⁸⁵, on Innate Lymphoid Cells Type 2 (ILC2s), which
405 signal back through IL-4 and IL-13 to the epithelium to aid worm clearance.^{81,83,84,86} IL17RA/B
406 expression has not previously been reported in hISCs, suggesting a novel role for IL25 signaling in
407 hISCs.

408 Under 24 hours of hypoxia, hISCs demonstrate less active progression through the cell cycle
409 and lower organoid forming efficiency. hISCs show increased stem cell activity in response to IL6, IL10,
410 and IL13, regardless of hypoxic conditioning. On the other hand, hypoxia induces hISCs to respond to
411 IL1 β , IL2, IL4, and IL25 by increasing stem cell activity in a hypoxia-dependent fashion. IL2 and IL4
412 promote cell survival effects by stimulating the Akt-pathway⁸⁷, and although there are fewer clear links
413 between IL25 (IL17RA/B) and cell survival, the IL17RA/B receptors can stimulate NF- κ B activation^{88,89},
414 which has cell survival effects under some stress stimuli.⁹⁰ While hypoxia alone can stimulate NF- κ B
415 activation through HIF1 α ^{8,91}, IL25 could amplify NF- κ B activation to increase hISC survival during
416 severe and prolonged hypoxic episodes. Interestingly, IL2, IL4, and IL25 stimulated increases in G2/M
417 in hISCs under hypoxia, with no change seen in hISCs under normoxia. G2/M arrest or delay by these
418 three cytokines might protect cells from undergoing checkpoint-induced cell death as the completion of
419 cytokinesis could be compromised by the lack of energetic and metabolic resources under severe
420 hypoxia.⁹² While many ILs have cell cycle effects on hISCs under normoxia, we see that many of these
421 effects change and produce novel responses that are only seen in the context of hypoxia. As such, it
422 appears hypoxia-primed hISCs likely respond differently to immune stimuli than normoxic hISCs, laying
423 the foundation for studies into unique, hypoxia-dependent genetic and biochemical mechanisms, which
424 preserve and restore hISC activity during and after hypoxic injury.

425 We acknowledge that deconstruction of the complex microenvironment of the in vivo human
426 stem cell niche limits some physiological interpretations. However, second generation studies using
427 our MPS can build on the findings of this study to test complex mixtures of hypoxia-related cytokines,
428 interactions of multiple cell types, and tunable O₂ concentrations to more accurately model and study
429 hISC behaviors under inflammatory hypoxia, more acute forms of oxygen deprivation, and clinically
430 relevant reperfusion. Previous iterations of the MPS have shown the ability of the MPS to dynamically
431 'reperfuse' hypoxic cultures with O₂, enabling studies of other modes cell death, such as ferroptosis,
432 which likely have a role in reperfusion injury due to reactive oxygen species production^{26,93,94}, or
433 pyroptosis, which are relevant to inflammasome-mediated cell death and are complex to model as they
434 involve microbes and immune cell components.^{95,96} As such the MPS is currently being optimized for
435 co-culture of hISCs, immune cells, and anaerobic commensal or pathological microbiota with the goal
436 of creating a more physiologically relevant environment to explore many facets that impact hISC
437 function and behavior.

MATERIALS AND METHODS

Primary human crypt isolation and intestinal epithelial stem cell culture

A surgical specimen of human small intestine (jejunum) was obtained from a donor at UNC Hospitals with consent of the patient (under the approved protocol UNC IRB #14- 2013). Villi and crypts were detached from the specimen by incubation in a chelating buffer for 75 min at 20°C followed by vigorous shaking in a 50 mL conical tube. The chelating buffer was composed of EDTA (2 mM), dithiothreitol (DTT, 0.5 mM, freshly added), Na₂HPO₄ (5.6 mM), KH₂PO₄ (8.0 mM), NaCl (96.2 mM), KCl (1.6 mM), sucrose (43.4 mM), D-sorbitol (54.9 mM), pH 1/4 7.4.⁹⁷ Released crypts were expanded as a monolayer on a neutralized collagen hydrogel as described previously.²⁵ Briefly, crypts were placed on the top of 1.0 mg/mL collagen hydrogels (1 ml into each well of 6-well plate (T1006; Denville, Holliston, MA)) at a density of 5,000 crypts/ well and overlaid with 4 ml of Expansion Media (EM) containing 10 mmol/L Y-27632 (S1049; SelleckChem). EM contains a mixture of advanced Dulbecco's modified Eagle medium/F12 medium (12634010; ThermoFisher) and Wnt-3A, R-spondin 3, noggin (WRN) conditioned medium (WRN medium prepared in lab from L-WRN cells (CRL- 3276; ATCC) following a published protocol⁹⁸ at a volumetric ratio of 1:1, and supplemented with GlutaMAX (35050061; ThermoFisher), B27 supplement without vitamin A (12587010; ThermoFisher), 10 mM HEPES (15630-080; ThermoFisher), 1.25 mM N-acetyl cysteine (194603; MP Bio, Santa Ana, CA), 10 mM nicotinamide (N0636; Sigma-Aldrich), 50 ng/mL epidermal growth factor (315-09; Peprotech), 2.0 nM gastrin (AS-64149; Anaspec), 10 nM prostaglandin E2 (14010; Cayman Chemicals), 3.0 μM SB202190 (S1077; Selleckchem), 100 U/mL penicillin-streptomycin (15140122; ThermoFisher), and 50 mg/mL primocin (ant-pm-1; InvivoGen, San Diego, CA). EM was used to expand the epithelial cell numbers as monolayers or organoids. Y-27632 was present only in the first 48 hours of cell culture and was not added to subsequent media changes. The medium was changed every 48 hours. When the cell coverage was greater than 80% (typically 5 to 7 days), the epithelium was dissociated to fragments to seed onto the intestinal MPS.

Fabrication of primary human intestinal microphysiological system (MPS)

The human intestinal MPS was fabricated from polymethylmethacrylate (PMMA) and photocured resin (Formlabs, Inc.). PMMA provided an optically transparent material with a low oxygen diffusion coefficient that could be sterilized and reused.⁹⁹ The photocured resin provided a 3D printable bottom frame to support the PMMA device and simultaneously house the optical reader for oxygen measurements. The cell culture chamber and gas exchange channels were fabricated from 5.8 mm and 1.5 mm-thick PMMA sheets (44352, 44292; US Plastics). The microfluidic culture region was composed of 5 rectangular wells, with dimensions of 11.6 mm by 7.0 mm each. The rectangular gas channel on top of the wells was 70 mm by 45 mm by 1.5 mm. The bottom and top pieces of PMMA were laser cut from a 1.5 mm-thick PMMA sheet, while the middle piece, for the cell culture wells, was laser cut from a 5.8 mm-thick PMMA sheet. Briefly, to remove dust and burr material with minimal cracking, each PMMA surface was quickly wiped with 100% IPA solution and air-dried. All 3 pieces were pressed together between two sheets of brass using a pneumatic heat press (SwingPress 10-0403; Across International). Annealing was performed with the heat press set at 100°C and 300 psi for 2 hours, then the bonded device was cooled for 3 hours at room temperature. A rubber gasket was laser cut and placed on top of the PMMA layer to seal the device, prior to bolting together. The device was tested for leaks using red and blue dyed water and cracks were sealed by application of dichloromethane (DCM) to the seams.

481 In the completed device, barbed connectors screwed into the photopolymer resin top lid provide
482 gas flow into and out of the device. A rubber gasket seals gas flow into and out of the PMMA gas
483 exchange channel. The gas exchange channel frame is bonded to the PMMA culture chamber and
484 PMMA base support. A photopolymer resin bottom frame supports the entire PMMA device, and screws
485 attach the top lid to the bottom frame to seal the MPS closed. The optics front-end connects via a
486 μ USB-to-HDMI cord to a phosphorescence-lifetime fluorimeter detector and interrogates the middle
487 culture well, where the iPOB is located.

488 A neutralized collagen hydrogel (2.0 mg/ml) was cast into each well of a prefabricated PMMA
489 device and allowed to polymerize at 37°C for 1 hour. 250 μ L of 1X DPBS was overlaid on the
490 polymerized hydrogel and allowed to pre-swell for at least 5 hours at room temperature. DPBS was
491 removed and the hydrogel was rinsed three times before overlaying with 250 μ L of EM containing hISCs
492 that had been mechanically dissociated by pipetting 10 times until cells were \sim 1-10 cell-clumps. Once
493 the hISCs formed a confluent monolayer, an iPOB was added to the epithelium to measure oxygen.

494 ***Real-time monitoring and control of oxygen concentration in 3D culture***

495 Oxygen concentration in the system was continuously measured with an integrated
496 phosphorescent oxygen sensor (iPOB) using near infrared (NIR) phosphorescence lifetime fluorimetry.
497 The iPOB is composed of porous poly(2-hydroxyethyl methacrylate) (pHEMA) gel functionalized with
498 palladium-benzoporphyrin derivatives (Pd-BPD) that respond to local oxygen concentrations via
499 phosphorescence quenching.²⁷ The photoluminescence excitation and detection wavelengths are 630
500 nm and 800 nm, respectively. The iPOB (Profusa, Inc., San Francisco, CA) has been manufactured in
501 a variety of sizes, but for all experiments a disk-shaped, 5 mm diameter and 0.5 mm thickness, iPOB
502 was used. The optics front-end of the NIR phosphorescence lifetime fluoroscope (Profusa, Inc., San
503 Francisco, CA) was inserted into the support frame below the MPS. The oxygen concentration was
504 controlled via a PMMA gas-mixing microfluidic chip with tubing connecting outlets from the gas-mixing
505 chip to the inlets of each MPS (**Fig 9A,B**). The gas-mixing chip was previously used to generate 8
506 concentrations of mixed gas, ranging from less than 3 μ M of oxygen to 180 μ M. (**Fig 9C,D**)²⁸ Gas flow
507 to the gas-mixing chip was regulated using an air flow control valve (62005K313; McMaster-Carr) and
508 monitored with a mass flow meter with digital output (GFMS-010061; Aalborg GFM) (**Fig 9B, Left**).
509 Hydrated mixed gas exiting the gas-mixing chip was introduced into individual MPS at a rate of 5
510 mL/min to prevent media evaporation. Within 30 minutes, the gas mixture equilibrated with the local
511 MPS environment to generate the desired oxygen concentration at the hydrogel surface-media
512 interface where oxygen was measured using the iPOB (**Fig. 1D**). The intestinal epithelium inside MPS
513 was cultured in the mixed gas environment and compared to intestinal epithelium statically cultured in
514 a normobaric incubator with an oxygen environment of 186 μ M.

515 ***Immunocytochemistry***

516 To assess the impact of various durations and magnitudes of hypoxia on hISC proliferation,
517 primary human intestinal epithelium and single cells isolated from each MPS chamber were stained for
518 Ki-67. For Ki-67 staining of intestinal epithelium following hypoxia, the intestinal MPS was opened, and
519 media was removed from each chamber. Intestinal epithelium on top of the collagen hydrogels were
520 fixed with 4% PFA for 15 minutes. After fixation, samples were rinsed once with 1X PBS and overlaid
521 with PBS. Samples were permeabilized for 15 minutes with 0.5% Triton-X 100 in 1X PBS. Samples
522 were blocked for 30 minutes with a 3% BSA solution. After blocking, samples were stained for
523 proliferation marker Ki-67 Alexa Fluor 647 (1:250 dilution in 3% BSA, Cat. No. 652407; BioLegend) for

1 hour and nuclei counterstain bisbenzimidazole (1:1000 dilution in 1X dPBS, Cat. No. 1155; Millipore Sigma) for 5 minutes at room temperature. To look at cell-cell contacts, tight junction protein Occludin (Cat. No. 13409-1-AP; Proteintech) was added for 1 hour, followed by incubator with the secondary antibody Cy3 (Cat. No. C2306; Sigma) for 2 hours. After staining, the gels were overlaid with 1X dPBS and stored at 4°C until imaging. All samples were imaged with a Olympus (Waltham, MA) IX81 microscope, using Metamorph Basic (Molecular Devices, San Jose, CA) software, and image analysis was performed with ImageJ.¹⁰⁰

Organoid forming efficiency assay and Fluorescence-activated cell sorting (FACS) of live cells

Following MPS culture, human intestinal epithelium was dissociated into single cells, sorted using a flow cytometer, and suspended in Matrigel[®] on a quad CellRaft[™] Array (CRA) platform (Cell Microsystems, Durham, NC).³⁴ Briefly, each sample was retrieved and placed in a separate conical. 500 U/mL Collagenase IV (17104019; Gibco) was added to breakdown the scaffold and incubated for 10 minutes at 37°C. After centrifugation, the cell pellet was rinsed twice in DPBS and re-suspended in 150 µL of 0.5 mmol/L EDTA in DPBS with 10 mmol/L Y-27632 and incubated for 5 minutes at 37°C. The fragments were further dispersed by triturating 30 times using a 200 µL pipet tip. After centrifugation, the cell pellet was re-suspended in 500 µL TrypLE Express (12605-036; Gibco) with 10 mmol/L Y-27632 and incubated for 5 minutes at 37°C. The cell suspension was gently triturated 7 times using a 28.5-gauge insulin needle to further dissociate. 500 µL of EM was added to quench the reaction, and cells were pelleted and rinsed once in EM. After pelleting again, cells were re-suspended in 200 µL of EM containing 1% FBS. Immediately before FACS, APC Annexin V (1:200, 640941; BioLegend) was added to cells for live/dead discrimination. After staining, cells were rinsed in EM and filtered through 0.4 µm FACS tube top filter (352235; Corning). 5,000 Annexin V- live cells were isolated via FACS and re-suspended in 250 µL of Growth Factor Reduced Matrigel[®] (354230; Corning). Cell-gel suspensions were plated in each chamber of the quad CRA. To cover the CRA, each array was centrifuged at 200 x g for 5 minutes. CRAs were polymerized for 20 minutes at 37°C in an incubator and then overlaid with EM containing 10 mmol/L Y-27632. Media was replaced every 2 days. To determine OFE, the CRA was scanned, and the total number of organoids was counted on day 2, day 4, and day 6. The OFE (%) was calculated as the total number of organoids created in one CRA chamber, divided by 5,000 cells and multiplied by 100. FACS and flow cytometry were performed using a SH800Z Cell Sorter (Sony Biotechnology, San Jose, CA).

Flow cytometry

Cells collected from normoxic and hypoxic MPS were dissociated following the protocol above up to the step of addition of TrypLE Express. Following trituration with the insulin needle and quenching with the EM, cells were pelleted and re-suspended in 100 µL of 1X DPBS. Approximately 50,000 cells from each chamber were fixed by adding 400 µL of 4% PFA solution while being constantly vortexed to prevent cell aggregation. After fixation, single cells were pelleted and re-suspended in 0.3% Triton-X for 15 minutes to permeabilize the cell membrane. Single cells were pelleted and re-suspended in a staining solution of DMEM containing 1% FBS and anti-Ki-67 Alex Fluor 647 (1:250 dilution in 3% BSA, Cat. No. 652407; BioLegend) for 1 hour on ice. After staining, cells were rinsed in PBS and filtered through 0.4 µm FACS tube top filter (352235; Corning). Ki-67-positive single cells were quantified by flow cytometry.

565 **qRT-PCR**

566 To assess the expression of genes that are responsive to hypoxia, human intestinal epithelial
567 samples from each MPS were collected for qRT-PCR analysis. Briefly, cells attached to collagen
568 hydrogels were lysed in 200 μ L of RNA Lysis buffer (AM1931; ThermoFisher). Total RNA was extracted
569 using RNAqueous-Micro Total RNA Isolation Kit (AM1931; ThermoFisher) according to manufacturer's
570 protocols. cDNA was generated from \sim 2 ng of total RNA from each sample using iScript Reverse
571 Transcription Supermix for qRT-PCR (170-8891; BioRad) according to manufacturer's protocols. cDNA
572 was diluted 1:20 and 1 μ L was used for qRT-PCR using the following Taqman probes:
573 HIF1 α :Hs00153153_m1, BNIP3: Hs00969289_m1, SLC2A1 (GLUT1): Hs00892681_m1, VEGFA:
574 Hs00900055_m1, IL6R: Hs01075664_m1, IL10RB: Hs00175123_m1, IL17RB: Hs00218889_m1,
575 IL22RA1: Hs00222035_m1 (Applied Biosystems) and SsoAdvanced Universal Probes Supermix
576 (1725281; BioRad) according to manufacturer's protocols. qRT-PCR was carried out in a StepOnePlus
577 Real Time PCR System (Applied Biosystems). For each sample and experiment, triplicates were made
578 and normalized to 18S mRNA levels. Fold change was expressed relative to normoxic controls using
579 $\Delta\Delta$ CT analysis.¹⁰¹ All statistics for gene expression were generated using a Student's t-test. In all
580 statistical analysis, $p < 0.05$ was considered significant.

581 **Bulk RNA-sequencing**

582 To investigate the dynamic response of hISC to hypoxia at the whole transcriptomic level, we
583 performed RNA-seq on human intestinal epithelium exposed to 6 hours, 24 hours, or 48 hours of
584 hypoxia inside intestinal MPS, along with normoxic control intestinal MPS which were cultured for each
585 respective time point with no hypoxia exposure. RNA samples were collected from each intestinal MPS,
586 and Total RNA was extracted using RNAqueous-Micro Total RNA Isolation Kit (AM1931;
587 ThermoFisher) according to manufacturer's protocols and stored at -80°C . To assess RNA quality prior
588 to submission for sequencing, an RNA integrity number (RIN) was measured using the Agilent 2100
589 Bioanalyzer. After confirmation that each sample had a RIN of at least 8, integrated fluidic circuits (IFCs)
590 for gene expression and genotyping analysis were prepared using the AdvantaTM RNA-Seq NGS
591 Library Prep Kit for the Fluidigm JunoTM.

592 **Informatics**

593 Gene level expression was obtained through pseudo alignment of reads to human genome
594 GRCh38 using Kallisto.¹⁰² Principal component and sample correlation analysis were done with
595 Bioconductor packages Biobase, cluster and qvalue.¹⁰³ Expression values for plotting were obtained
596 by TMM normalization across all samples using EdgeR package and differential expression between
597 normoxic and hypoxic samples at each time point was calculated from raw counts with DESeq2.^{104,105}
598 GSEAs were performed using all hallmark gene sets on $n = 3$ samples from each duration of hypoxia
599 (6-, 24-, and 48-hours) to its corresponding normoxic control separately. These comparisons were
600 ranked by NES.^{106,107}

601 **ACKNOWLEDGEMENTS**

602 The authors would like to thank all the members of the Magness Laboratory, specifically Dr.
603 Meryem Ok, and the Biointerface Lab, along with Drs. Michael Gamcsik and Bailey Zwarycz for helpful
604 discussions. The authors thank the Center for Gastrointestinal Biology and Disease (CGIBD) and the
605 CGIBD's Advanced Analytics Core under NIH grant P30 DK034987. This work was done in
606 collaboration with the National Science Foundation (EEC-1160483) through a

607 NSF Nanosystems Engineering Research Center (NERC) for Advanced Self-Powered Systems of
608 Integrated Sensors and Technologies (ASSIST), CCSS-1846911 (M.D.) and CBE/EBS-2033997 (M.D.,
609 S.T.M.). K.R.R. was supported by the National Institutes of Health under award number
610 F31DK118859-02, the 2019 Howard Hughes Medical Institute Gilliam Fellowship Award,
611 F32DK124929 (J.R.B.), R01DK109559 (S.T.M.), the Katherine E. Bullard Charitable Trust for
612 Gastrointestinal Stem Cell and Regenerative Research (S.T.M.), and CGIBD Pilot & Feasibility Award
613 P30 DK034987 (M.D./S.T.M.). We thank Gabrielle Cannon at the Advanced Analytics core at UNC
614 Chapel Hill.

615 **AUTHOR CONTRIBUTIONS**

616 K.R.R. designed the study and conducted the experiments, analyzed data, and wrote the manuscript.
617 R.J.B. conducted experiments, analyzed RNA sequencing results, and wrote the manuscript
618 M.J.C. conducted experiments and analyzed RNA sequencing results.
619 J.B. conducted experiments, helped analyze data, and reviewed the manuscript
620 J.L. conducted experiments and analyzed data
621 J.M.T. conducted experiments
622 C.M.H. helped analyze data
623 K.A.B. helped analyze data
624 S.J. conducted experiments
625 V.A.P. worked with K.R.R. to build and integrate all components of the microphysiological systems.
626 M.Y. designed, fabricated, and validated the gas mixing chip using COMSOL Multiphysics and
627 experimental methods.
628 M.D. and S.T.M. conceived the study and wrote the manuscript.
629 A.Z. Contributed experimental design and informatics analysis
630 A.T.B. Provided intellectual contributions on the topics of mechanisms of ischemia/reperfusion and
631 hypoxic injury

632 **CONFLICT OF INTEREST**

633 STM has a financial interest in Altis Biosystems, Inc., Durham, NC. The remaining authors declare no
634 competing related financial interests or conflict of interest at the time of the conduct of this study.

635 **FIGURE CAPTIONS**

636 **Figure 1. Development of a tunable hypoxic microphysiological system (MPS) with integrated**
637 **oxygen sensors and cultured primary human intestinal epithelium.**

638 **A)** Exploded view of MPS compartments. **B)** (left) Top view photograph of a standard microscope glass
639 slide (75 x 25 mm) and dime, for reference, placed above the MPS with iPOB (black arrow) inside well
640 3 and red and blue dyes in wells 1 and 5 and 2 and 4, respectively. (middle) 1 well brightfield image of
641 monolayer of cells. (right) Inset from 1 well brightfield image shows magnified colonies in hISC
642 monolayer. **C)** (Top) Side view photograph of MPS with middle well containing the green iPOB.
643 Schematic of iPOB integrated into hydrogel to measure oxygen at the cell layer inside the cell culture

well. (Bottom-left) Schematic of porphyrin-based luminescence. In high oxygen, luminescence from the porphyrin is quenched by energy transfer to oxygen, resulting in a decrease in phosphorescence lifetime. In the absence of oxygen, porphyrin molecules are excited by LED from the detector and phosphoresce with increased lifetime. **D**) Plots of 8 oxygen concentration versus time (7.5 hours) measurements from the iPOB inside the MPS, with 8 different mixed gas inputs, show generation of 8 established oxygen environments. **E**) (Top-left) Brightfield image of human intestinal epithelial stem and progenitor cells grown inside a MPS well to confluence. Fluorescent images show tight junction structures between epithelial cells marked by the protein Occludin (magenta, bottom-right), stem cells marked by SOX9 (magenta, top-right, and proliferative cells marked by EdU (red, bottom). Nuclei are marked by Bisbenzimidazole staining in grey or blue. **F**) Organoid forming efficiency (%) measured over 6 days from single cells isolated from MPS after 5 days in culture. **G**) Oxygen concentration tracked using the iPOB inside a MPS containing human intestinal epithelium for 24 hours with normoxic and hypoxic culture environments.

Figure 2. Primary human intestinal epithelium cultured under hypoxia inside microphysiological system shows dynamic response to different durations of hypoxia

A) Representative images showing colonies of human intestinal stem cells cultured on collagen scaffolds as 2D monolayers showing dynamic changes in HIF1 α IF staining over different durations of normoxia or acute hypoxia. **B**) Mean pixel intensity of HIF1 α staining in **A** over different durations of normoxia or hypoxia. Technical replicates represent mean pixel intensities of all nuclei in 3 individual colonies. **C**) RT-qPCR results of human intestinal epithelium for downstream HIF1 α targets (BNIP3, GLUT1, VEGFA) after 24 hours of normoxic or hypoxic environment exposure. **D**) Flow cytometry results from single cells isolated after 6, 24, 48, and 72 hours from normoxic and hypoxic MPS and stained for Annexin V(-) to quantify cell viability cells (%) **E**) Immunostaining of hISC monolayer colonies for proliferation marker KI67 following 24 or 48 hours of hypoxia **F**) Functional stemness as measured by Organoid forming efficiency (OFE %) for 24-hour normoxic and hypoxic samples after 6-days of 3D MatrigelTM-embedded culture. **G**) Functional stemness for 48-hour normoxic and hypoxic samples after 6-day of 3D MatrigelTM-embedded culture. **H**) Principal component analysis of RNA-seq results showing clusters of replicate samples from each time point (6, 24, 48 hours) and condition (normoxia or hypoxia). Bulk RNA-sequencing samples were sequenced from a range of 39 to 93 million reads **I**) Heatmap showing mean CPM-normalized and log-transformed expression of stem/progenitor markers or differentiated lineage markers from hypoxia bulk RNA sequencing in **2H**.

Figure 3. Characterizing the transcriptomic response to different durations of hypoxia by primary human intestinal epithelium

A) Hallmark GSEA results for differentially expressed genes at each time point of hypoxia shown compared to normoxic controls. DEGs from RNAseq from each timepoint from **2H** were compared using GSEA and ranked by Normalized Enrichment Score. Gene sets related to hypoxia or inflammatory signaling are highlighted in pink. **B**) Heatmaps of gene expression from bulk RNAseq data from **2H** for all genes from the Hallmark Inflammatory Response GSEA gene expressed in the bulk data set. Interleukin receptors from the Hallmark Inflammatory Response gene set that are expressed in our dataset are highlighted in pink.

Figure 4. Hypoxia-induced changes in hISC gene expression for interleukin receptors

685 **A-C**). Fold change comparison of expressed IL receptor genes from each duration of hypoxia in **2H** is
686 shown. Differentially expressed genes that are upregulated in hypoxia compared to their normoxic
687 counter parts are shown above 1 and genes downregulated in hypoxia are shown below 1. Pink dots
688 signify genes that are significantly upregulated in hypoxia at a given timepoint and blue dots represent
689 genes that are significantly downregulated in hypoxia at a given time point. Grey dots represent IL
690 receptor genes that are not significantly differentially expressed at a given time point. Text lists genes
691 represented by the colored dots sorted by descending fold change. **D**) qRT-PCR measured after 24
692 hours of normoxia or hypoxia for IL receptor genes that are consistently up- or down-regulated at either
693 6, 24, or 48 hours of hypoxia. **E**) Dot plot showing DEG interleukin receptors from (**A-C**) and hISC and
694 proliferation marker genes from hISC and TA cells from scRNAseq data of primary human intestinal
695 epithelium. **F**) Dot plot showing DEG interleukin receptors from (**A-C**) and hISC and proliferation marker
696 genes from hISC and TA cells from scRNAseq data of in vitro primary hISC and progenitors.

697 **Figure 5. Severe hypoxia increases proportion of hISCs residing in G1 phase**

698 **A**) Experimental schematic to assess impact of hypoxia and interleukins on cell cycle progression in
699 human intestinal epithelial cells. **B**) Example of raw confocal imaging data showing Bisbenzimidazole+
700 nuclei (top), Cellpose segmented nuclei mask, (second from top), EdU (second from bottom), and KI67
701 (bottom). **C**) Example of mitotic bodies found in KI67 channel. **D**) Histogram showing distribution of
702 normalized KI67 mean pixel intensities across Normoxic and Hypoxic conditions without interleukin
703 treatments. Table shows key descriptive statistics that highlight statistically significant differences in
704 distributions. **** $p < 0.0001$ by Kolgorov-Smirnov test of cumulative distributions. **E**) Percent of KI67⁺,
705 EdU⁺, and Mitotic Bodies counted per colony in normoxia and hypoxia conditions without treatment
706 from interleukins. Dots represent per-colony averages of single-cell mean-pixel intensity values from
707 separate normoxic or hypoxic colonies.

708 **Figure 6. Severe hypoxia primes hISCs to respond differently to regulation of cell cycle by** 709 **interleukins**

710 **A**) Quantification of cell cycle progression metrics from **5E** for hISCs treated with 24 hours of normoxia
711 or hypoxia with or without IL1 α . **B**) Quantification of cell cycle progression metrics from **5E** for hISCs
712 treated with 24 hours of normoxia or hypoxia with or without IL1 β . **C**) Quantification of cell cycle
713 progression metrics from **5E** for hISCs treated with 24 hours of normoxia or hypoxia with or without IL2.
714 **D**) Quantification of cell cycle progression metrics from **5E** for hISCs treated with 24 hours of normoxia
715 or hypoxia with or without IL4. **E**) Quantification of cell cycle progression metrics from **5E** for hISCs
716 treated with 24 hours of normoxia or hypoxia with or without IL25. **F**) Quantification of cell cycle
717 progression metrics from **54E** for hISCs treated with 24 hours of normoxia or hypoxia with or without
718 IL22.

719 **Figure 7. Interleukins with no significant effect on hISCs regardless of oxygen condition**

720 **A**) Quantification of cell cycle progression metrics from **5E** for hISCs treated with 24 hours of normoxia
721 or hypoxia with or without IL6. **B**) Quantification of cell cycle progression metrics from **5E** for hISCs
722 treated with 24 hours of normoxia or hypoxia with or without IL10. **C**) Quantification of cell cycle
723 progression metrics from **5E** for hISCs treated with 24 hours of normoxia or hypoxia with or without
724 IL13. **D**) Quantification of cell cycle progression metrics from **5E** for hISCs treated with 24 hours of
725 normoxia or hypoxia with or without IL17^{A/F}.

Figure 8. hISCs demonstrate hypoxia-dependent rescue of organoid forming efficiency when treated with specific interleukins

A) Experimental schematic to assess impact of hypoxia, then reoxygenation and interleukins on functional stem cell activity. **B)** Impact of hypoxia and reoxygenation on functional stem cell activity without treatment of interleukins. **C)** Representative images of organoids from conditions in **B,D-M**. Images have been pseudocolored to highlight outer membranes of organoids. **D)** Impact of hypoxia and reoxygenation plus IL6 from on functional stem cell activity. **E)** Impact of hypoxia and reoxygenation plus IL10 from on functional stem cell activity. **F)** Impact of hypoxia and reoxygenation plus IL13 from on functional stem cell activity. **G)** Impact of hypoxia and reoxygenation plus IL1 β from on functional stem cell activity. **H)** Impact of hypoxia and reoxygenation plus IL2 from on functional stem cell activity. **I)** Impact of hypoxia and reoxygenation plus IL4 from on functional stem cell activity. **J)** Impact of hypoxia and reoxygenation plus IL25 from on functional stem cell activity. **K)** Impact of hypoxia and reoxygenation plus IL1 α from on functional stem cell activity. **L)** Impact of hypoxia and reoxygenation plus IL17^{AF} from on functional stem cell activity. **M)** Impact of hypoxia and reoxygenation plus IL22 from on functional stem cell activity.

Figure 9. Gas mixing chip integrated into microphysiological system to generate 8 different oxygen environments.

A) Schematic of complete microphysiological system design with mixed gases in tanks leading into flow meters. Flow meters connect into humidification 15 mL conical tube filled with sterile PBS. Humidified gases travel into each input of the gas mixer chip, and 8 concentrations of gases exit individual outlets to connect into separate microphysiological systems (devices). Device oxygen concentration is monitored using detectors that send information to a laptop located beside the incubator. **B)** Images taken of each component of the system. **C)** COMSOL Multiphysics results for the simulated gas mixtures from each outlet of the gas mixing chip. **D)** Image of the gas mixing chip and measured output oxygen concentrations recorded inside individual devices.

REFERENCES

- 1 Carreau, A., El Hafny-Rahbi, B., Matejuk, A., Grillon, C. & Kieda, C. Why is the partial oxygen pressure of human tissues a crucial parameter? Small molecules and hypoxia. *Journal of cellular and molecular medicine* **15**, 1239-1253 (2011). <https://doi.org/10.1111/j.1582-4934.2011.01258.x>
- 2 Espey, M. G. Role of oxygen gradients in shaping redox relationships between the human intestine and its microbiota. *Free Radical Biology and Medicine* **55**, 130-140 (2013). <https://doi.org/10.1016/j.freeradbiomed.2012.10.554>
- 3 Zheng, L., Kelly, C. J. & Colgan, S. P. Physiologic hypoxia and oxygen homeostasis in the healthy intestine. A Review in the Theme: Cellular Responses to Hypoxia. *American journal of physiology. Cell physiology* **309**, C350-C360 (2015). <https://doi.org/10.1152/ajpcell.00191.2015>
- 4 Taylor, C. T. & Colgan, S. P. Regulation of immunity and inflammation by hypoxia in immunological niches. *Nature Reviews Immunology* **17**, 774-785 (2017). <https://doi.org/10.1038/nri.2017.103>
- 5 Li, G., Wang, S. & Fan, Z. Oxidative Stress in Intestinal Ischemia-Reperfusion. *Front Med (Lausanne)* **8**, 750731 (2021). <https://doi.org/10.3389/fmed.2021.750731>
- 6 Gonzalez, L. M., Moeser, A. J. & Bliklager, A. T. Animal models of ischemia-reperfusion-induced intestinal injury: progress and promise for translational research. *American journal of physiology. Gastrointestinal and liver physiology* **308**, G63-G75 (2015). <https://doi.org/10.1152/ajpgi.00112.2013>

- 768 7 Saxena, K. & Jolly, M. K. Acute vs. Chronic vs. Cyclic Hypoxia: Their Differential Dynamics, Molecular Mechanisms,
769 and Effects on Tumor Progression. *Biomolecules* **9** (2019). <https://doi.org/10.3390/biom9080339>
- 770 8 Van Welden, S., Selfridge, A. C. & Hindryckx, P. Intestinal hypoxia and hypoxia-induced signalling as therapeutic
771 targets for IBD. *Nat Rev Gastroenterol Hepatol* **14**, 596-611 (2017). <https://doi.org/10.1038/nrgastro.2017.101>
- 772 9 Shah, Y. M. The role of hypoxia in intestinal inflammation. *Mol Cell Pediatr* **3**, 1 (2016).
773 <https://doi.org/10.1186/s40348-016-0030-1>
- 774 10 Eltzschig, H. K. & Carmeliet, P. Hypoxia and inflammation. *New England Journal of Medicine* **364**, 656-665 (2011).
775 11 Campbell, L., Eric *et al.* Transmigrating Neutrophils Shape the Mucosal Microenvironment through Localized
776 Oxygen Depletion to Influence Resolution of Inflammation. *Immunity* **40**, 66-77 (2014).
777 <https://doi.org/10.1016/j.immuni.2013.11.020>
- 778 12 Eltzschig, H. K., Bratton, D. L. & Colgan, S. P. Targeting hypoxia signalling for the treatment of ischaemic and
779 inflammatory diseases. *Nat Rev Drug Discov* **13**, 852-869 (2014). <https://doi.org/10.1038/nrd4422>
- 780 13 Colgan, S. P., Furuta, G. T. & Taylor, C. T. Hypoxia and Innate Immunity: Keeping Up with the HIFsters. *Annual*
781 *Review of Immunology* **38**, 341-363 (2020). <https://doi.org/10.1146/annurev-immunol-100819-121537>
- 782 14 Colgan, S. P. & Taylor, C. T. Hypoxia: an alarm signal during intestinal inflammation. *Nature reviews.*
783 *Gastroenterology & hepatology* **7**, 281-287 (2010). <https://doi.org/10.1038/nrgastro.2010.39>
- 784 15 Guan, Y., Worrell, R. T., Pritts, T. A. & Montrose, M. H. Intestinal ischemia-reperfusion injury: reversible and
785 irreversible damage imaged in vivo. *American journal of physiology. Gastrointestinal and liver physiology* **297**,
786 G187-G196 (2009). <https://doi.org/10.1152/ajpgi.90595.2008>
- 787 16 Cartwright, I. M. & Colgan, S. P. The hypoxic tissue microenvironment as a driver of mucosal inflammatory
788 resolution. *Frontiers in Immunology* **14**, 116
- 789 17 Blikslager, A. T., Roberts, M. C., Rhoads, J. M. & Argenzio, R. A. Is reperfusion injury an important cause of mucosal
790 damage after porcine intestinal ischemia? *Surgery* **121**, 526-534 (1997). [https://doi.org/10.1016/s0039-6060\(97\)90107-0](https://doi.org/10.1016/s0039-6060(97)90107-0)
- 791 18 Blikslager, A. T., Roberts, M. C., Rhoads, J. M. & Argenzio, R. A. Prostaglandins I2 and E2 have a synergistic role in
792 rescuing epithelial barrier function in porcine ileum. *J Clin Invest* **100**, 1928-1933 (1997).
793 <https://doi.org/10.1172/JCI119723>
- 794 19 Leenarts, C. A. *et al.* Histopathology of human small intestinal and colonic ischemia-reperfusion: Experiences from
795 human IR-models. *Histol Histopathol* **34**, 711-722 (2019). <https://doi.org/10.14670/HH-18-074>
- 796 20 Grootjans, J. *et al.* Human intestinal ischemia-reperfusion-induced inflammation characterized: experiences from
797 a new translational model. *The American journal of pathology* **176**, 2283-2291 (2010).
798 <https://doi.org/10.2353/ajpath.2010.091069>
- 799 21 Hundscheid, I. H. *et al.* The Human Colon Is More Resistant to Ischemia–reperfusion–induced Tissue Damage Than
800 the Small Intestine. *Annals of Surgery* **262**, 304-311 (2015). <https://doi.org/10.1097/sla.0000000000001131>
- 801 22 Gonzalez, L. M. *et al.* Preservation of reserve intestinal epithelial stem cells following severe ischemic injury.
802 *American journal of physiology. Gastrointestinal and liver physiology* **316**, G482-G494 (2019).
803 <https://doi.org/10.1152/ajpgi.00262.2018>
- 804 23 Singleton, D. C., Macann, A. & Wilson, W. R. Therapeutic targeting of the hypoxic tumour microenvironment. *Nat*
805 *Rev Clin Oncol* **18**, 751-772 (2021). <https://doi.org/10.1038/s41571-021-00539-4>
- 806

- 24 Derikx, J. P. M. *et al.* Rapid Reversal of Human Intestinal Ischemia-Reperfusion Induced Damage by Shedding of Injured Enterocytes and Reepithelialisation. *PLoS ONE* **3**, e3428 (2008). <https://doi.org/10.1371/journal.pone.0003428>
- 25 Wang, Y. *et al.* Self-renewing Monolayer of Primary Colonic or Rectal Epithelial Cells. *Cellular and Molecular Gastroenterology and Hepatology* **4**, 165-182.e167 (2017). <https://doi.org/10.1016/j.jcmgh.2017.02.011>
- 26 Rivera, K. R. *et al.* Integrated phosphorescence-based photonic biosensor (iPOB) for monitoring oxygen levels in 3D cell culture systems. *Biosensors & Bioelectronics* **123**, 131-140 (2019). <https://doi.org/10.1016/j.bios.2018.07.035>
- 27 Wisniewski, N. A. *et al.* Tissue-Integrating Oxygen Sensors: Continuous Tracking of Tissue Hypoxia. *Advances in experimental medicine and biology* **977**, 377-383 (2017). https://doi.org/10.1007/978-3-319-55231-6_49
- 28 Yao, M. *et al.* Mixing and delivery of multiple controlled oxygen environments to a single multiwell culture plate. *American journal of physiology. Cell physiology* **315**, C766-C775 (2018). <https://doi.org/10.1152/ajpcell.00276.2018>
- 29 Hinman, S. S., Wang, Y., Kim, R. & Allbritton, N. L. In vitro generation of self-renewing human intestinal epithelia over planar and shaped collagen hydrogels. *Nature Protocols* **16**, 352-382 (2021). <https://doi.org/10.1038/s41596-020-00419-8>
- 30 Formeister, E. J. *et al.* Distinct SOX9 levels differentially mark stem/progenitor populations and enteroendocrine cells of the small intestine epithelium. *American journal of physiology. Gastrointestinal and liver physiology* **296**, G1108-G1118 (2009). <https://doi.org/10.1152/ajpgi.00004.2009>
- 31 Gracz, A. D., Ramalingam, S. & Magness, S. T. Sox9 expression marks a subset of CD24-expressing small intestine epithelial stem cells that form organoids in vitro. *American Journal of Physiology. Gastrointestinal and Liver Physiology* **298**, G590-600 (2010). <https://doi.org/10.1152/ajpgi.00470.2009>
- 32 Sato, T. & Clevers, H. Growing Self-Organizing Mini-Guts from a Single Intestinal Stem Cell: Mechanism and Applications. *Science* **340**, 1190-1194 (2013). <https://doi.org/10.1126/science.1234852>
- 33 Wang, Y. *et al.* Capture and 3D culture of colonic crypts and colonoids in a microarray platform. *Lab on A Chip* **13**, 4625-4634 (2013). <https://doi.org/10.1039/c3lc50813g>
- 34 Gracz, A. D. *et al.* A high-throughput platform for stem cell niche co-cultures and downstream gene expression analysis. *Nature Cell Biology* **17**, 340-349 (2015). <https://doi.org/10.1038/ncb3104>
- 35 Gjorevski, N. *et al.* Designer matrices for intestinal stem cell and organoid culture. *Nature* **539**, 560-564 (2016). <https://doi.org/10.1038/nature20168>
- 36 Ebbesen, E. O. P. J. P. Hypoxia, Normoxia and Hyperoxia: Terminology for Medical In Vitro Cell Biology. *Acta Oncologica* **39**, 247-248 (2000). <https://doi.org/10.1080/028418600430888>
- 37 Taylor, C. T. & Colgan, S. P. Hypoxia and gastrointestinal disease. *Journal of Molecular Medicine* **85**, 1295-1300 (2007). <https://doi.org/10.1007/s00109-007-0277-z>
- 38 Semenza, G. L. HIF-1, O₂, and the 3 PHDs. *Cell* **107**, 1-3 (2001). [https://doi.org/10.1016/s0092-8674\(01\)00518-9](https://doi.org/10.1016/s0092-8674(01)00518-9)
- 39 Wang, Y. *et al.* Long-Term Culture Captures Injury-Repair Cycles of Colonic Stem Cells. *Cell* **179**, 1144-1159.e1115 (2019). <https://doi.org/10.1016/j.cell.2019.10.015>
- 40 Huang, L. E., Arany, Z., Livingston, D. M. & Bunn, H. F. Activation of Hypoxia-inducible Transcription Factor Depends Primarily upon Redox-sensitive Stabilization of Its α Subunit. *Journal of Biological Chemistry* **271**, 32253-32259 (1996). <https://doi.org/10.1074/jbc.271.50.32253>

- 347 41 Gradin, K. *et al.* Functional interference between hypoxia and dioxin signal transduction pathways: competition
348 for recruitment of the Arnt transcription factor. *Molecular and Cellular Biology* **16**, 5221-5231 (1996).
349 <https://doi.org/10.1128/MCB.16.10.5221>
- 350 42 Forsythe, J. A. *et al.* Activation of vascular endothelial growth factor gene transcription by hypoxia-inducible factor
351 1. *Mol Cell Biol* **16**, 4604-4613 (1996). <https://doi.org/10.1128/MCB.16.9.4604>
- 352 43 Ebert, B. L., Firth, J. D. & Ratcliffe, P. J. Hypoxia and Mitochondrial Inhibitors Regulate Expression of Glucose
353 Transporter-1 via Distinct Cis-acting Sequences. *Journal of Biological Chemistry* **270**, 29083-29089 (1995).
354 <https://doi.org/10.1074/jbc.270.49.29083>
- 355 44 Kothari, S. *et al.* BNIP3 plays a role in hypoxic cell death in human epithelial cells that is inhibited by growth factors
356 EGF and IGF. *Oncogene* **22**, 4734-4744 (2003). <https://doi.org/10.1038/sj.onc.1206666>
- 357 45 Koopman, G. *et al.* Annexin V for flow cytometric detection of phosphatidylserine expression on B cells undergoing
358 apoptosis. *Blood* **84**, 1415-1420 (1994). <https://doi.org/10.1182/blood.v84.5.1415.1415>
- 359 46 Stern, A. *et al.* The CellRaft AIR[®] system: A novel system enabling organoid imaging, identification, and isolation.
360 *SLAS Discovery* **27**, 201-208 (2022). <https://doi.org/10.1016/j.slasd.2021.11.003>
- 361 47 Breau, K. A. *et al.* Efficient transgenesis and homology-directed gene targeting in monolayers of primary human
362 small intestinal and colonic epithelial stem cells. *Stem Cell Reports* **17**, 1493-1506 (2022).
363 <https://doi.org/10.1016/j.stemcr.2022.04.005>
- 364 48 Burclaff, J. *et al.* A Proximal-to-Distal Survey of Healthy Adult Human Small Intestine and Colon Epithelium by
365 Single-Cell Transcriptomics. *Cellular and Molecular Gastroenterology and Hepatology* **13**, 1554-1589 (2022).
366 <https://doi.org/10.1016/j.jcmgh.2022.02.007>
- 367 49 Carbon, S. *et al.* AmiGO: online access to ontology and annotation data. *Bioinformatics (Oxford, England)* **25**, 288-
368 289 (2009). <https://doi.org/10.1093/bioinformatics/btn615>
- 369 50 Hung, J.-H., Yang, T.-H., Hu, Z., Weng, Z. & Delisi, C. Gene set enrichment analysis: performance evaluation and
370 usage guidelines. *Briefings in Bioinformatics* **13**, 281-291 (2012). <https://doi.org/10.1093/bib/bbr049>
- 371 51 Benczik, M. & Gaffen, S. L. The interleukin (IL)-2 family cytokines: survival and proliferation signaling pathways in
372 T lymphocytes. *Immunol Invest* **33**, 109-142 (2004). <https://doi.org/10.1081/imm-120030732>
- 373 52 Bersudsky, M. *et al.* Non-redundant properties of IL-1alpha and IL-1beta during acute colon inflammation in mice.
374 *Gut* **63**, 598-609 (2014). <https://doi.org/10.1136/gutjnl-2012-303329>
- 375 53 Bischoff, S. C. *et al.* IL-4 enhances proliferation and mediator release in mature human mast cells. *Proc Natl Acad*
376 *Sci U S A* **96**, 8080-8085 (1999). <https://doi.org/10.1073/pnas.96.14.8080>
- 377 54 Chen, J., Wang, Y., Shen, L., Xiu, Y. & Wang, B. Could IL-25 be a potential therapeutic target for intestinal
378 inflammatory diseases? *Cytokine Growth Factor Rev* (2022). <https://doi.org/10.1016/j.cytogfr.2022.07.001>
- 379 55 Dorransoro, A. *et al.* Intracellular role of IL-6 in mesenchymal stromal cell immunosuppression and proliferation.
380 *Scientific Reports* **10** (2020). <https://doi.org/10.1038/s41598-020-78864-4>
- 381 56 Jenkins, S. J. *et al.* IL-4 directly signals tissue-resident macrophages to proliferate beyond homeostatic levels
382 controlled by CSF-1. *J Exp Med* **210**, 2477-2491 (2013). <https://doi.org/10.1084/jem.20121999>
- 383 57 Junttila, I. S. Tuning the Cytokine Responses: An Update on Interleukin (IL)-4 and IL-13 Receptor Complexes.
384 *Frontiers in immunology* **9**, 888 (2018). <https://doi.org/10.3389/fimmu.2018.00888>
- 385 58 Friedrich, M., Pohin, M. & Powrie, F. Cytokine Networks in the Pathophysiology of Inflammatory Bowel Disease.
386 *Immunity* **50**, 992-1006 (2019). <https://doi.org/10.1016/j.immuni.2019.03.017>

- 887 59 Andrews, C., McLean, M. H. & Durum, S. K. Cytokine Tuning of Intestinal Epithelial Function. *Front Immunol* **9**,
888 1270 (2018). <https://doi.org/10.3389/fimmu.2018.01270>
- 889 60 Neurath, M. F. Cytokines in inflammatory bowel disease. *Nat Rev Immunol* **14**, 329-342 (2014).
890 <https://doi.org/10.1038/nri3661>
- 891 61 Gomez-Martinez, I. *et al.* A Planar Culture Model of Human Absorptive Enterocytes Reveals Metformin Increases
892 Fatty Acid Oxidation and Export. *Cellular and Molecular Gastroenterology and Hepatology* **14**, 409-434 (2022).
893 <https://doi.org/10.1016/j.jcmgh.2022.04.009>
- 894 62 Stringer, C. & Pachitariu, M. Cellpose 2.0: how to train your own model. *bioRxiv* (2022).
- 895 63 Stringer, C., Wang, T., Michaelos, M. & Pachitariu, M. Cellpose: a generalist algorithm for cellular segmentation.
896 *Nat Methods* **18**, 100-106 (2021). <https://doi.org/10.1038/s41592-020-01018-x>
- 897 64 Miller, I. *et al.* Ki67 is a Graded Rather than a Binary Marker of Proliferation versus Quiescence. *Cell Reports* **24**,
898 1105-1112.e1105 (2018). <https://doi.org/10.1016/j.celrep.2018.06.110>
- 899 65 Malkov, M. I., Lee, C. T. & Taylor, C. T. Regulation of the Hypoxia-Inducible Factor (HIF) by Pro-Inflammatory
900 Cytokines. *Cells* **10** (2021). <https://doi.org/10.3390/cells10092340>
- 901 66 Mao, Y.-M. *et al.* Interleukin-13: A promising therapeutic target for autoimmune disease. *Cytokine & growth factor*
902 *reviews* **45**, 9-23 (2019). <https://doi.org/10.1016/j.cytogfr.2018.12.001>
- 903 67 McLean, M. H., Neurath, M. F. & Durum, S. K. Targeting interleukins for the treatment of inflammatory bowel
904 disease-what lies beyond anti-TNF therapy? *Inflamm Bowel Dis* **20**, 389-397 (2014).
905 <https://doi.org/10.1097/01.MIB.0000437616.37000.41>
- 906 68 Li, L. J., Gong, C., Zhao, M. H. & Feng, B. S. Role of interleukin-22 in inflammatory bowel disease. *World J*
907 *Gastroenterol* **20**, 18177-18188 (2014). <https://doi.org/10.3748/wjg.v20.i48.18177>
- 908 69 Ziegler, A. L. *et al.* Epithelial restitution defect in neonatal jejunum is rescued by juvenile mucosal homogenate in
909 a pig model of intestinal ischemic injury and repair. *PLOS ONE* **13**, e0200674 (2018).
910 <https://doi.org/10.1371/journal.pone.0200674>
- 911 70 Ziegler, A., Gonzalez, L. & Blikslager, A. Large Animal Models: The Key to Translational Discovery in Digestive
912 Disease Research. *Cellular and molecular gastroenterology and hepatology* **2**, 716-724 (2016).
913 <https://doi.org/10.1016/j.jcmgh.2016.09.003>
- 914 71 Grootjans, J. *et al.* Level of activation of the unfolded protein response correlates with Paneth cell apoptosis in
915 human small intestine exposed to ischemia/reperfusion. *Gastroenterology* **140**, 529-539.e523 (2011).
916 <https://doi.org/10.1053/j.gastro.2010.10.040>
- 917 72 Kip, A. M. *et al.* Temporal Transcript Profiling Identifies a Role for Unfolded Protein Stress in Human Gut Ischemia-
918 Reperfusion Injury. *Cell Mol Gastroenterol Hepatol* **13**, 681-694 (2022).
919 <https://doi.org/10.1016/j.jcmgh.2021.11.001>
- 920 73 Bartoszewska, S. & Collawn, J. F. Unfolded protein response (UPR) integrated signaling networks determine cell
921 fate during hypoxia. *Cell Mol Biol Lett* **25**, 18 (2020). <https://doi.org/10.1186/s11658-020-00212-1>
- 922 74 Livezey, M., Huang, R., Hergenrother, P. J. & Shapiro, D. J. Strong and sustained activation of the anticipatory
923 unfolded protein response induces necrotic cell death. *Cell Death Differ* **25**, 1796-1807 (2018).
924 <https://doi.org/10.1038/s41418-018-0143-2>
- 925 75 Saveljeva, S., Mc Laughlin, S. L., Vandenabeele, P., Samali, A. & Bertrand, M. J. Endoplasmic reticulum stress
926 induces ligand-independent TNFR1-mediated necroptosis in L929 cells. *Cell Death Dis* **6**, e1587 (2015).
927 <https://doi.org/10.1038/cddis.2014.548>

- 928 76 Bankaitis, E. D., Ha, A., Kuo, C. J. & Magness, S. T. Reserve stem cells in intestinal homeostasis and injury. *Gastroenterology* **155**, 1348-1361 (2018). <https://doi.org/10.1053/j.gastro.2018.08.016>
- 929
- 930 77 Moriggl, R. *et al.* Stat5 is required for IL-2-induced cell cycle progression of peripheral T cells. *Immunity* **10**, 249-259 (1999). [https://doi.org/10.1016/s1074-7613\(00\)80025-4](https://doi.org/10.1016/s1074-7613(00)80025-4)
- 931
- 932 78 Vella, A. T., Dow, S., Potter, T. A., Kappler, J. & Marrack, P. Cytokine-induced survival of activated T cells in vitro and in vivo. *Proc Natl Acad Sci U S A* **95**, 3810-3815 (1998). <https://doi.org/10.1073/pnas.95.7.3810>
- 933
- 934 79 Prokopchuk, O., Liu, Y., Henne-Bruns, D. & Kornmann, M. Interleukin-4 enhances proliferation of human pancreatic cancer cells: evidence for autocrine and paracrine actions. *Br J Cancer* **92**, 921-928 (2005). <https://doi.org/10.1038/sj.bjc.6602416>
- 935
- 936
- 937 80 Koller, F. L., Hwang, D. G., Dozier, E. A. & Fingleton, B. Epithelial interleukin-4 receptor expression promotes colon tumor growth. *Carcinogenesis* **31**, 1010-1017 (2010). <https://doi.org/10.1093/carcin/bgq044>
- 938
- 939 81 Gerbe, F. *et al.* Intestinal epithelial tuft cells initiate type 2 mucosal immunity to helminth parasites. *Nature* **529**, 226-230 (2016). <https://doi.org/10.1038/nature16527>
- 940
- 941 82 Gerbe, F., Legraverend, C. & Jay, P. The intestinal epithelium tuft cells: specification and function. *Cellular and Molecular Life Sciences* **69**, 2907-2917 (2012). <https://doi.org/10.1007/s00018-012-0984-7>
- 942
- 943 83 von Moltke, J., Ji, M., Liang, H.-E. & Locksley, R. M. Tuft-cell-derived IL-25 regulates an intestinal ILC2-epithelial response circuit. *Nature* **529**, 221-225 (2016). <https://doi.org/10.1038/nature16161>
- 944
- 945 84 Howitt, M. R. *et al.* Tuft cells, taste-chemosensory cells, orchestrate parasite type 2 immunity in the gut. *Science* **351**, 1329-1333 (2016). <https://doi.org/10.1126/science.aaf1648>
- 946
- 947 85 Rickel, E. A. *et al.* Identification of functional roles for both IL-17RB and IL-17RA in mediating IL-25-induced activities. *J Immunol* **181**, 4299-4310 (2008). <https://doi.org/10.4049/jimmunol.181.6.4299>
- 948
- 949 86 Smith, K. A. *et al.* Concerted IL-25R and IL-4R α signaling drive innate type 2 effector immunity for optimal helminth expulsion. *Elife* **7** (2018). <https://doi.org/10.7554/eLife.38269>
- 950
- 951 87 Lindemann, M. J., Benczik, M. & Gaffen, S. L. Anti-apoptotic signaling by the interleukin-2 receptor reveals a function for cytoplasmic tyrosine residues within the common gamma (γ c) receptor subunit. *J Biol Chem* **278**, 10239-10249 (2003). <https://doi.org/10.1074/jbc.M209471200>
- 952
- 953
- 954 88 Awane, M., Andres, P. G., Li, D. J. & Reinecker, H. C. NF-kappa B-inducing kinase is a common mediator of IL-17-, TNF-alpha-, and IL-1 beta-induced chemokine promoter activation in intestinal epithelial cells. *J Immunol* **162**, 5337-5344 (1999).
- 955
- 956
- 957 89 Chang, S. H., Park, H. & Dong, C. Act1 adaptor protein is an immediate and essential signaling component of interleukin-17 receptor. *J Biol Chem* **281**, 35603-35607 (2006). <https://doi.org/10.1074/jbc.C600256200>
- 958
- 959 90 Yang, C. H. *et al.* IFN α /beta promotes cell survival by activating NF-kappa B. *Proc Natl Acad Sci U S A* **97**, 13631-13636 (2000). <https://doi.org/10.1073/pnas.250477397>
- 960
- 961 91 D'Ignazio, L. & Rocha, S. Hypoxia Induced NF-kB. *Cells* **5** (2016). <https://doi.org/10.3390/cells5010010>
- 962
- 963 92 Hasvold, G. *et al.* Hypoxia-induced alterations of G2 checkpoint regulators. *Mol Oncol* **10**, 764-773 (2016). <https://doi.org/10.1016/j.molonc.2015.12.015>
- 964
- 965 93 Chen, Y. *et al.* Ferroptosis: A Novel Therapeutic Target for Ischemia-Reperfusion Injury. *Front Cell Dev Biol* **9**, 688605 (2021). <https://doi.org/10.3389/fcell.2021.688605>
- 966
- 967 94 Li, Y. *et al.* Ischemia-induced ACSL4 activation contributes to ferroptosis-mediated tissue injury in intestinal ischemia/reperfusion. *Cell Death Differ* **26**, 2284-2299 (2019). <https://doi.org/10.1038/s41418-019-0299-4>

- 968 95 Bergsbaken, T., Fink, S. L. & Cookson, B. T. Pyroptosis: host cell death and inflammation. *Nat Rev Microbiol* **7**, 99-
969 109 (2009). <https://doi.org/10.1038/nrmicro2070>
- 970 96 Wu, Y. *et al.* Cell pyroptosis in health and inflammatory diseases. *Cell Death Discov* **8**, 191 (2022).
971 <https://doi.org/10.1038/s41420-022-00998-3>
- 972 97 Sato, T. *et al.* Long-term expansion of epithelial organoids from human colon, adenoma, adenocarcinoma, and
973 Barrett's epithelium. *Gastroenterology* **141**, 1762-1772 (2011). <https://doi.org/10.1053/j.gastro.2011.07.050>
- 974 98 Miyoshi, H. & Stappenbeck, T. S. In vitro expansion and genetic modification of gastrointestinal stem cells in
975 spheroid culture. *Nature Protocols* **8**, 2471-2482 (2013). <https://doi.org/10.1038/nprot.2013.153>
- 976 99 Rivera, K. R., Yokus, M. A., Erb, P. D., Pozdin, V. A. & Daniele, M. Measuring and regulating oxygen levels in
977 microphysiological systems: design, material, and sensor considerations. *The Analyst* **144**, 3190-3215 (2019).
978 <https://doi.org/10.1039/c8an02201a>
- 979 100 Schneider, C. A., Rasband, W. S. & Eliceiri, K. W. NIH Image to ImageJ: 25 years of image analysis. *Nature Methods*
980 **9**, 671-675 (2012). <https://doi.org/10.1038/nmeth.2089>
- 981 101 Livak, K. J. & Schmittgen, T. D. Analysis of Relative Gene Expression Data Using Real-Time Quantitative PCR and
982 the 2- $\Delta\Delta$ CT Method. *Methods* **25**, 402-408 (2001). <https://doi.org/10.1006/meth.2001.1262>
- 983 102 Bray, N. L., Pimentel, H., Melsted, P. & Pachter, L. Near-optimal probabilistic RNA-seq quantification. *Nature*
984 *Biotechnology* **34**, 525-527 (2016). <https://doi.org/10.1038/nbt.3519>
- 985 103 Huber, W. *et al.* Orchestrating high-throughput genomic analysis with Bioconductor. *Nature methods* **12**, 115-121
986 (2015). <https://doi.org/10.1038/nmeth.3252>
- 987 104 Love, M. I., Huber, W. & Anders, S. Moderated estimation of fold change and dispersion for RNA-seq data with
988 DESeq2. *Genome biology* **15**, 550-550 (2014). <https://doi.org/10.1186/s13059-014-0550-8>
- 989 105 Robinson, M. D., McCarthy, D. J. & Smyth, G. K. edgeR: a Bioconductor package for differential expression analysis
990 of digital gene expression data. *Bioinformatics (Oxford, England)* **26**, 139-140 (2010).
991 <https://doi.org/10.1093/bioinformatics/btp616>
- 992 106 Mootha, V. K. *et al.* PGC-1alpha-responsive genes involved in oxidative phosphorylation are coordinately
993 downregulated in human diabetes. *Nat Genet* **34**, 267-273 (2003). <https://doi.org/10.1038/ng1180>
- 994 107 Subramanian, A. *et al.* Gene set enrichment analysis: a knowledge-based approach for interpreting genome-wide
995 expression profiles. *Proc Natl Acad Sci U S A* **102**, 15545-15550 (2005). <https://doi.org/10.1073/pnas.0506580102>
- 996

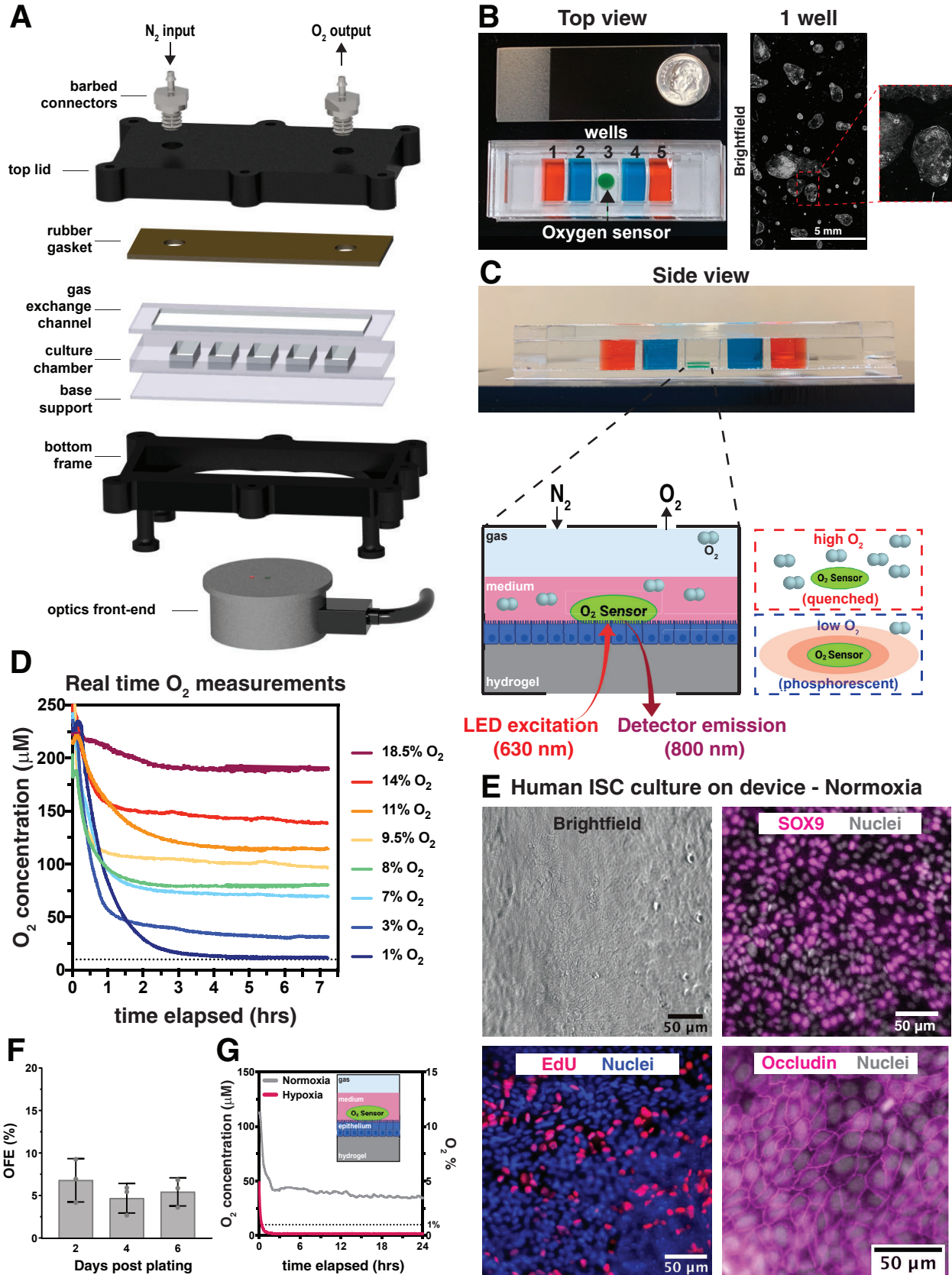


Figure 1

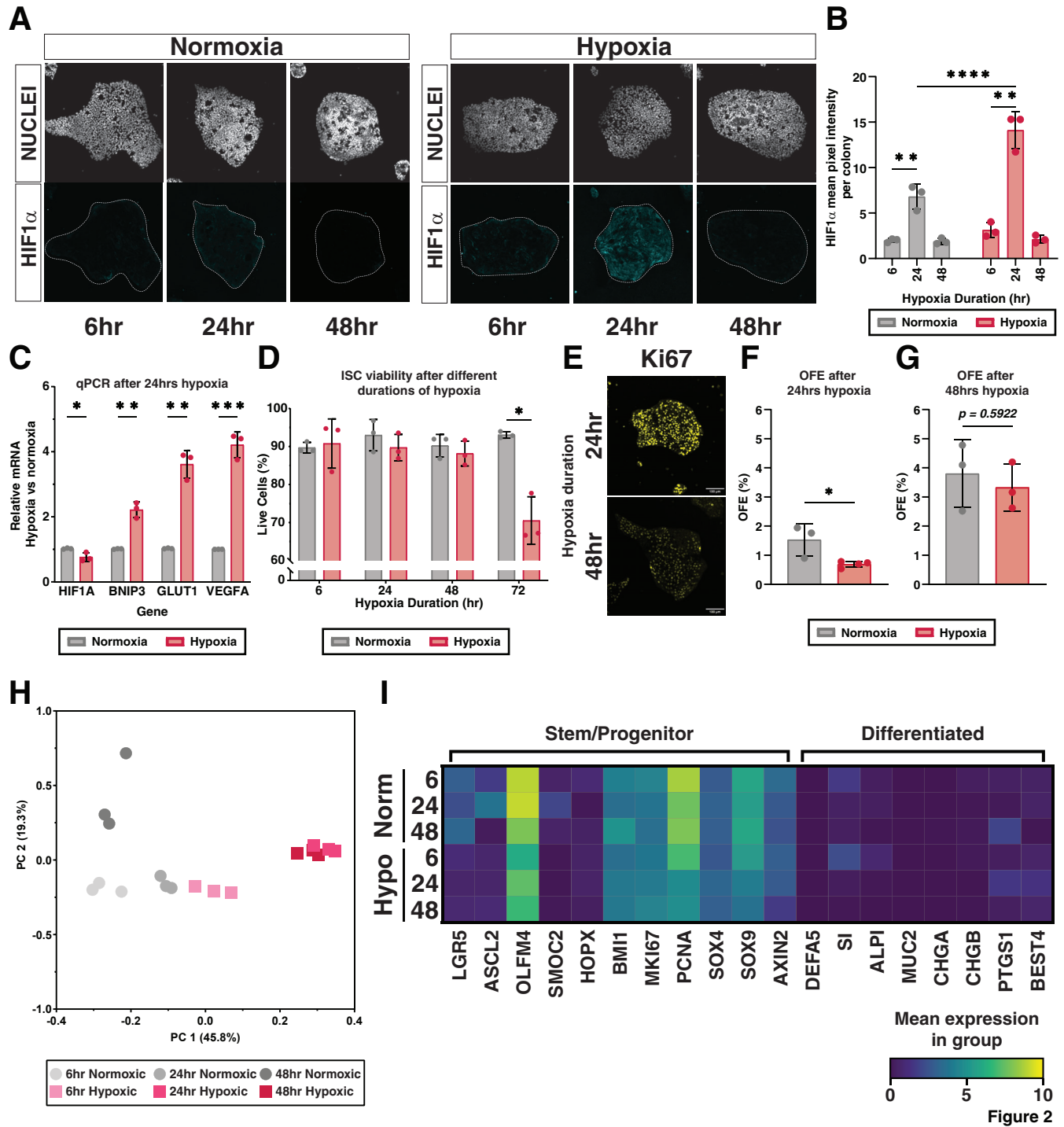
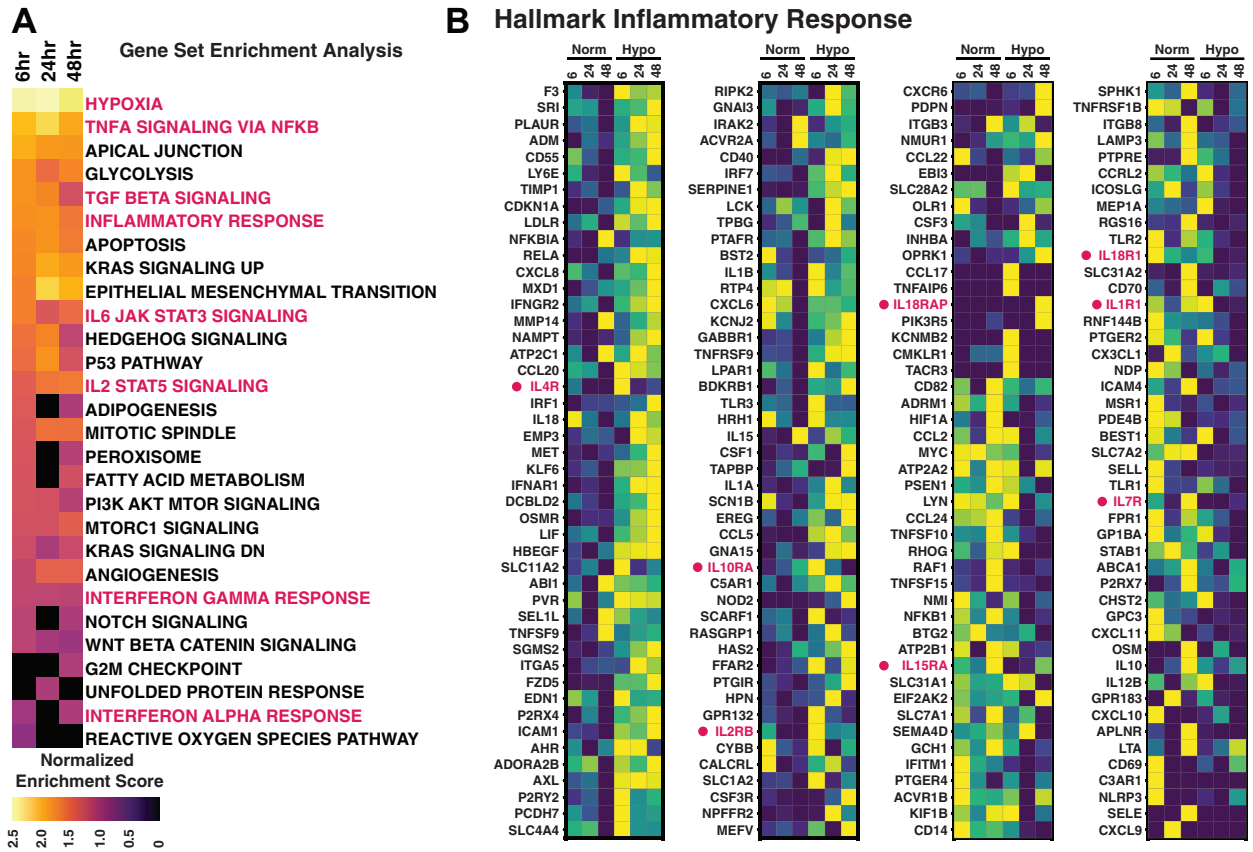


Figure 2



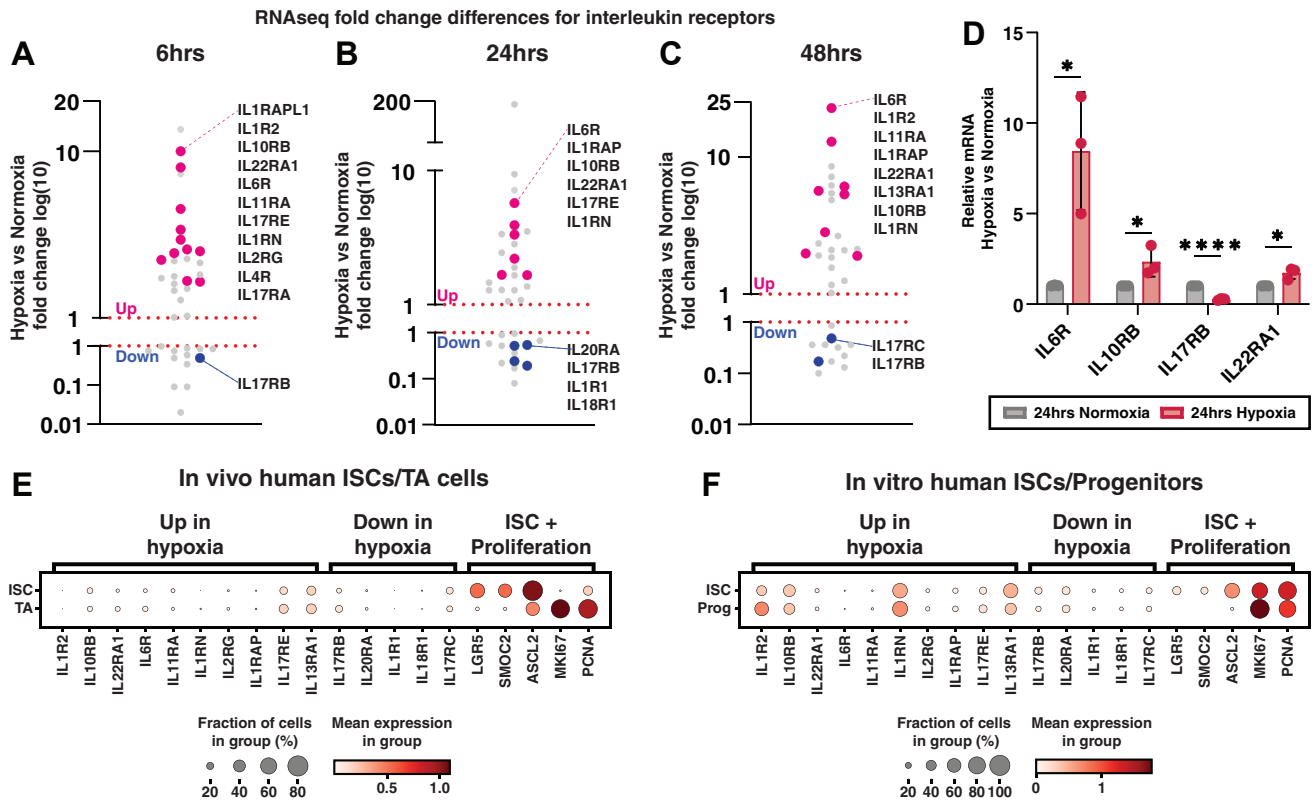


Figure 4

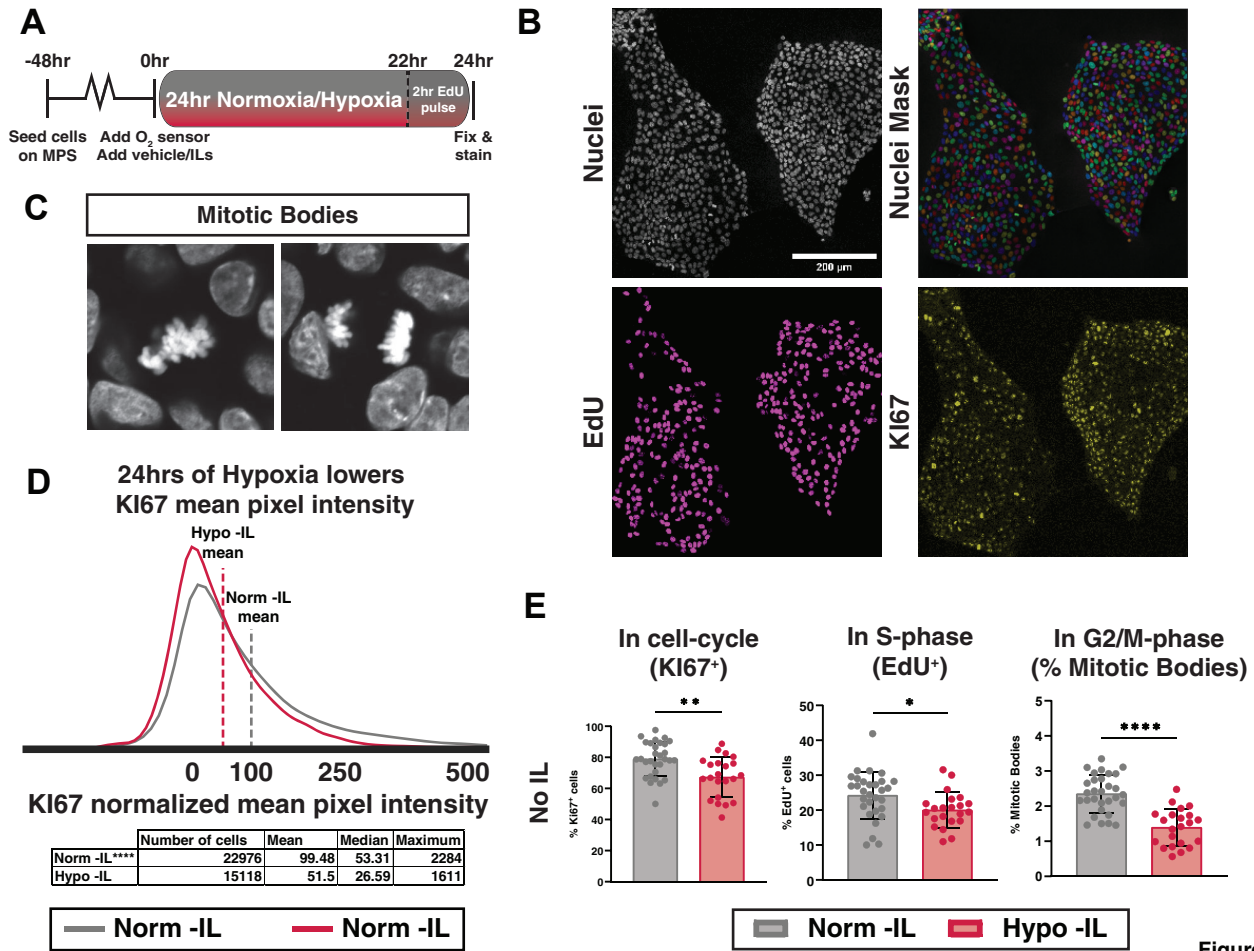


Figure 5

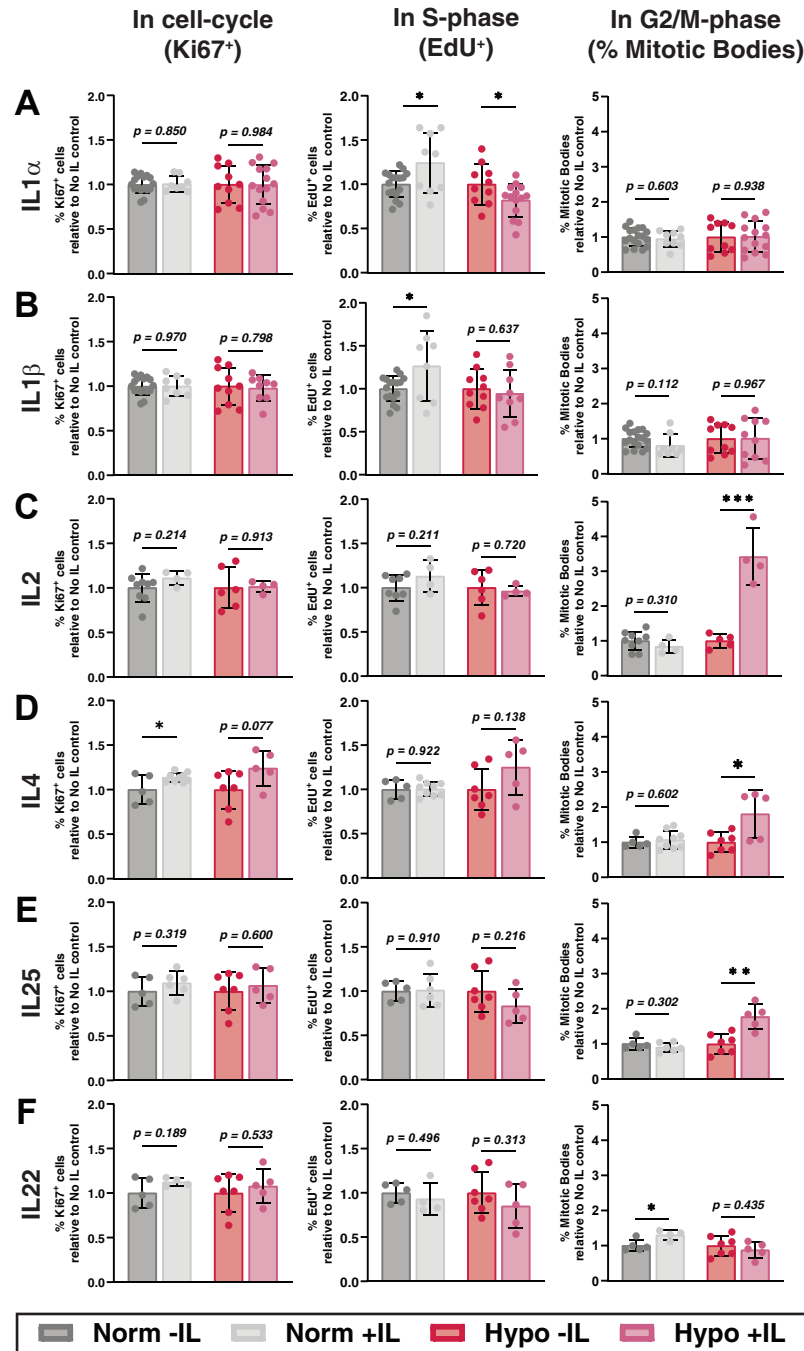


Figure 6

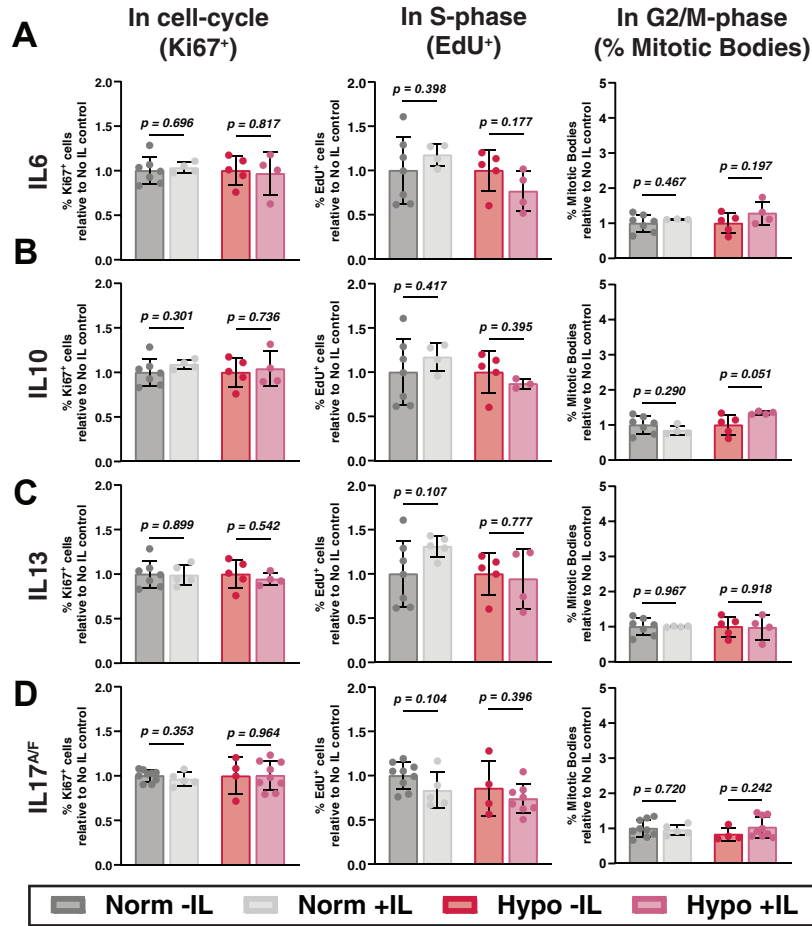


Figure 7

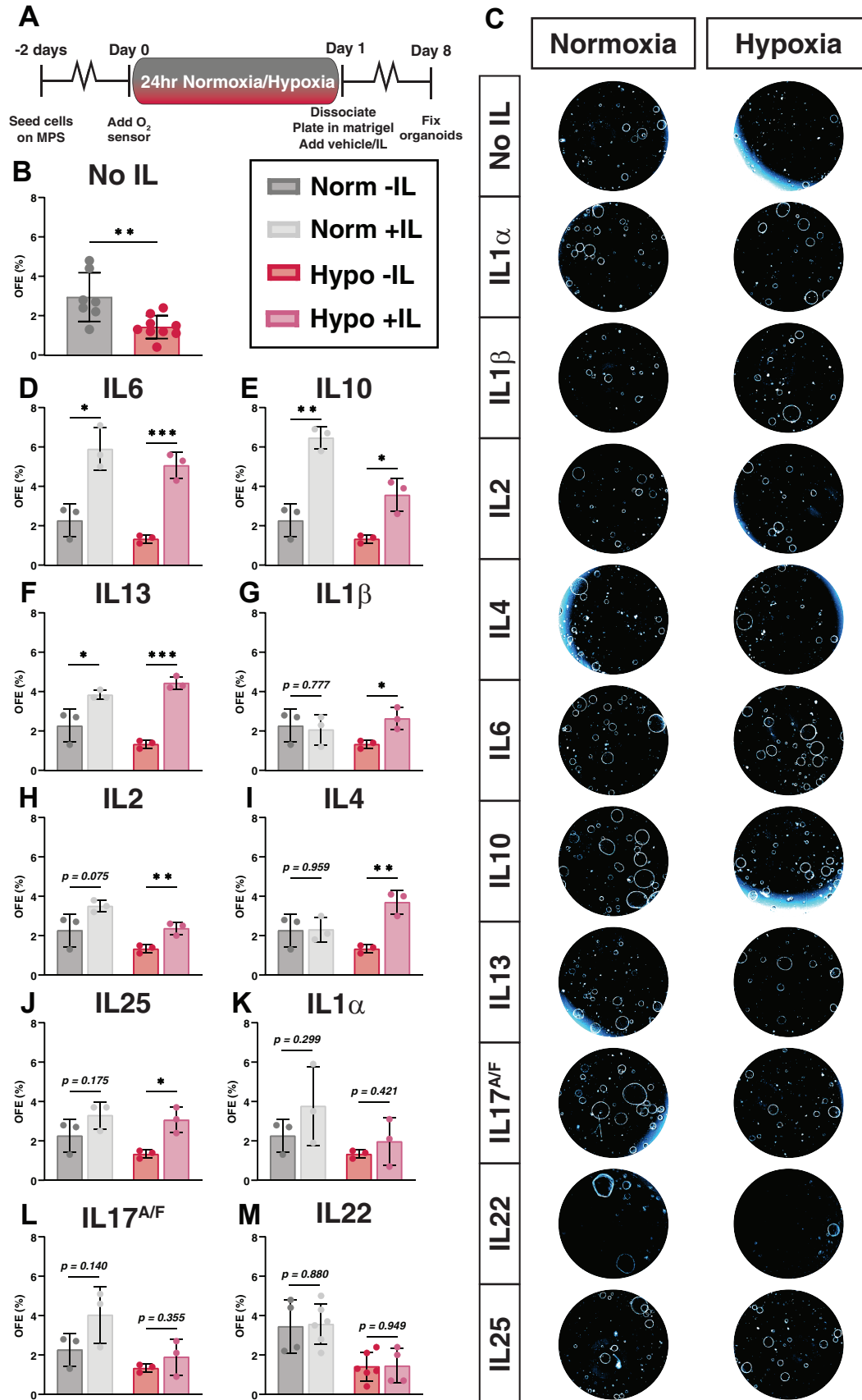


Figure 8

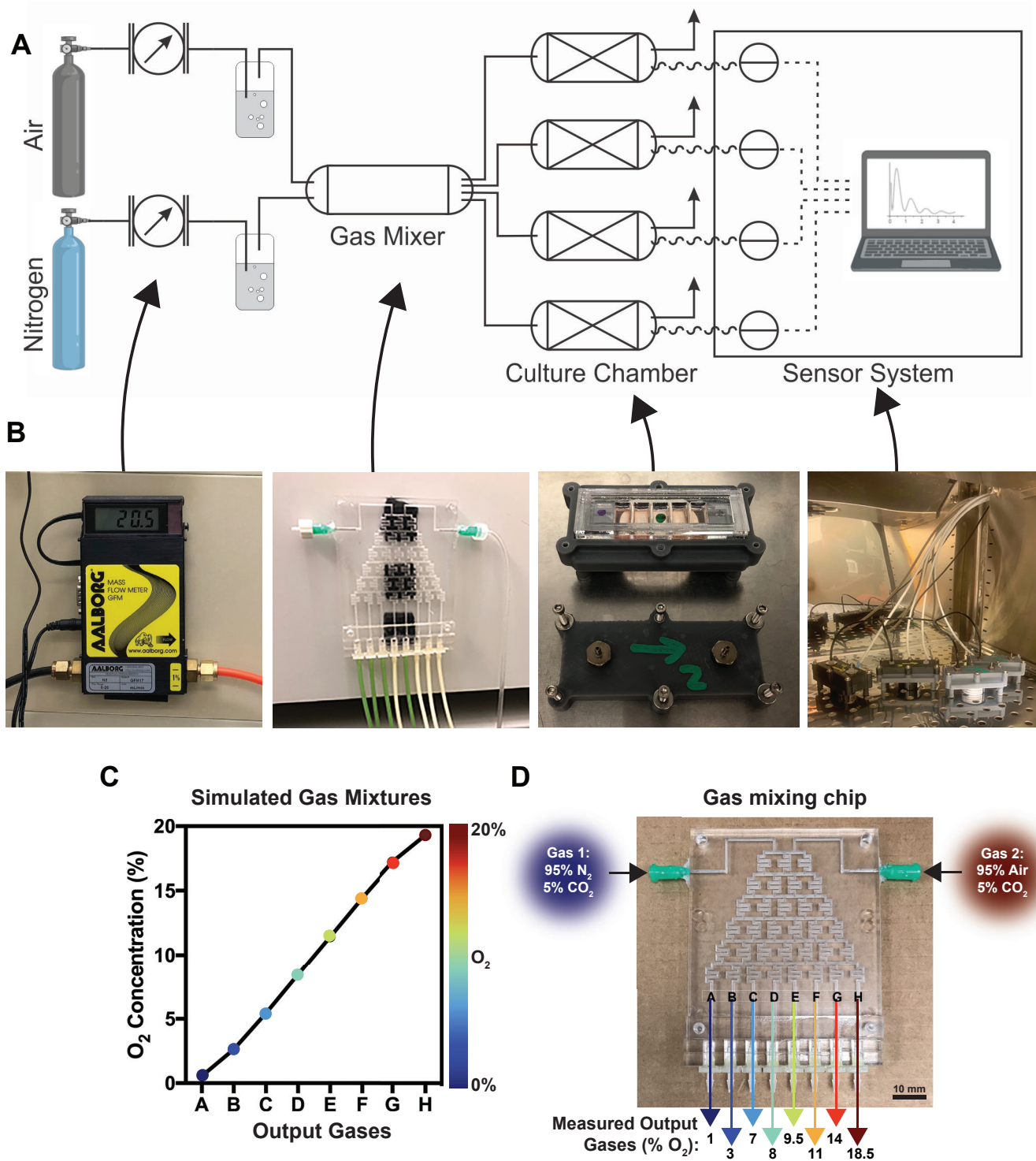


Figure 9